AFCRL-64-915

MODIFICATION TO THE SCATTERING BEHAVIOR OF A SPHERE BY REACTIVE LOADING

by

V. V. Liepa and T. B. A. Senior

October 1964

Scientific Report No. 2

Contract AF 19(628)-2374
Project 5635
Task 563502

Prepared for

Air Force Cambridge Research Laboratories
Office of Aerospace Research
L. G. Hanscom Field
Bedford, Massachusetts

TABLE OF CONTENTS

ABSTRACT

Electromagnetic scattering behavior by a metallic sphere loaded with a circumferential slot in the plane normal to the direction of incidence is investigated. The slot is assumed to be of small but non-zero width with electric field constant across it, and under this assumption the analysis of external field is exact. The field scattered in any direction is obtained by superposition of the field diffracted by an unloaded sphere and that radiated by an excited slot at the position of the load, with the radiation strength of the slot related to the loading characteristics in the combined problem. Thus, there are two parameters that determine the scattering behavior of this object: the loading admittance and the position of the slot.

Numerical results are presented primarily for the case of back scattering and these are compared with experimental measurements made using a metallic sphere with an equatorial slot backed by a radial cavity of adjustable depth.

I
INTRODUCTION

A major problem in scattering theory is the development of ways for controlling the scattering behavior of an object through modifications to its surface. It has long been recognized that minor shape changes can be effective in reducing (or even enhancing) the scattering cross section, primarily at high frequencies, and with the development of high performance absorbers during the past decade, the application of these materials has now become one of the most potent tools for cross section reduction. As the frequency is decreased, however, absorbers lose much of their utility. At wavelengths comparable to, or larger than, the overall dimensions of the scatterer, the thickness of any good non-resonant absorber is liable to be intolerable, and to achieve a reasonable degree of absorption the properties of the material must also be tailored to the individual shape parameters of the surface. This last severely complicates the problem of designing the material. It is therefore desirable to investigate other means of cross section control, particularly ones which are effective in the resonance region, and of these new techniques the most promising is that known as reactive loading.

In essence, the technique is to change the impedance "seen" by the incident field over a restricted portion of the surface using a cavity-backed slot, lumped network, or other type of microwave circuit, and as such is only a special case of the general theory of surface impedance effects. Mathematically at least, it is akin to the application of absorbers, but in practice differs both in the localized nature of the region where the loading is employed and in the greater variety of impedances that can be achieved either to enhance or decrease the scattered field.

The first reported application of this technique for cross section reduction was by Iams (1950), who used it to decrease the scattering from metallic posts in a parallel plate pillbox structure. King (1956) investigated the change in current on a thin cylindrical rod when a central load was introduced, and Hu (1958) and Ås and Schmitt (1958) later showed that loading can appreciably affect the scattering behavior of such a rod. However, it was not until the recent study by Chen and Liepa (1964) that the ultimate capability of loading for cross section reduction was fully demonstrated. For normal incidence on a thin cylinder of length ℓ, $0<\ell<2\lambda$, the induced current was calculated as a function of an arbitrary central load, and the results confirmed by detailed current measurements on a model. The back scattering cross section was then determined, and it was found that for every value of ℓ/λ within the chosen range, a loading exists for which the cross section is zero. The real and imaginary parts of the corresponding optimum impedances were obtained as functions of ℓ/λ, and whereas the required loading was passive when $\ell<\lambda$, that for $\lambda<\ell<2\lambda$ was primarily active.

Chen and Liepa also considered the scattering in directions other than normal to the surface, and in two later papers Chen (1964a and b) has extended the analysis to oblique incidence and to the case of two identical symmetrically-placed loads. Valuable as this work is, however, its usefulness for most applications is limited by the requirement that the cylinder be thin (radius much less than the wavelength), and though Sletten et al (1964) have shown experimentally that reactive loading is still effective when the cylinder is thick (radius comparable with the length), no theoretical treatment of this problem is yet available.

A somewhat different and more abstract approach to reactive loading is to represent the body as a one-port (Harrington, 1963; Green, 1963) or n-port (Weinberg, 1963; Harrington, 1964) device, which leads to the expression of the scattered field in terms of commonly-defined antenna parameters. However, to use the method to obtain quantitative results it is necessary to determine the transmitting and receiving properties of the body, and for an accurate treatment this again involves the solution of the boundary value problems.

The most simple example of a "thick" body is the sphere, and this is the shape that we shall consider here. A plane wave is assumed to impinge on a perfectly conducting sphere loaded in a narrow azimuthal region whose plane is normal to the direction of incidence. The field scattered in any direction can then be obtained by superposition of the field diffracted by an unloaded sphere and that radiated by an excited slot at the position of the load, with the radiation strength of the slot related to the loading characteristics in the combined problem. The concept of distributed admittances is introduced, and by varying the admittance Y_ℓ of the slot, a wide degree of control over the scattering behavior can be exercised. Even if attention is confined to passive loads (admittances whose real parts are non-negative), substantial increases or decreases in the scattered amplitude in almost any specified direction can be achieved by appropriate choice of Y_ℓ. Numerical results are presented, primarily for the case of back scattering, and these are compared with measurements made using a model with an equatorial slot backed by a cavity of adjustable depth. The agreement is excellent.

II
FIELD EXPRESSIONS

Consider first an unslotted perfectly conducting sphere of radius a whose center is at the origin of a Cartesian coordinate system (x, y, z). A plane electromagnetic wave is assumed incident in the direction of the negative z axis, and, since there is no loss of generality in taking its electric vector to lie in the x direction, we choose

$$\underline{E}^i = \hat{x}\, e^{ikz} \qquad \text{and} \qquad \underline{H}^i = -\hat{y}\, Y e^{ikz}$$

where Y is the intrinsic admittance of free space and a time factor $e^{i\omega t}$ has been suppressed.

If we also introduce the spherical polar coordinates (r, θ, ϕ) such that

$$x = r\sin\theta\cos\phi, \quad y = r\sin\theta\sin\phi, \quad z = r\cos\theta$$

with $\theta = 0$ representing the back scattering direction and $\theta = \pi$ the forward one, the above expressions for the incident field can be expanded in terms of the vector wave functions $\underline{M}^{(1)}$ and $\underline{N}^{(1)}$ in the form

$$\underline{E}^i = \sum_{n=1}^{\infty} i^n \frac{2n+1}{n(n+1)} \left(\underline{M}^{(1)}_{o1n} - i\,\underline{N}^{(1)}_{e1n} \right) \tag{1}$$

$$\underline{H}^i = iY \sum_{n=1}^{\infty} i^n \frac{2n+1}{n(n+1)} \left(\underline{N}^{(1)}_{o1n} - i\,\underline{M}^{(1)}_{e1n} \right) \tag{2}$$

(Stratton, 1941), where

$$\underline{M}^{(1)}_{\substack{e\\o}mn} = \mp m \frac{\psi_n(kr)}{kr} \frac{P_n^m(\cos\theta)}{\sin\theta} \begin{matrix}\sin\\ \cos\end{matrix} m\phi\,\hat{\theta} - \frac{\psi_n(kr)}{kr} \frac{\partial}{\partial\theta} P_n^m(\cos\theta) \begin{matrix}\cos\\ \sin\end{matrix} m\phi\,\hat{\phi}$$

$$\underline{N}^{(1)}_{\substack{e\\o}mn} = n(n+1)\,\frac{\psi_n(kr)}{(kr)^2}\,P_n^m(\cos\theta)\,{\cos \atop \sin} m\phi\,\hat{r} + \frac{\psi_n'(kr)}{kr}\,\frac{\partial}{\partial\theta}\,P_n^m(\cos\theta)\,{\cos \atop \sin} m\phi\,\hat{\theta}$$

$$\mp m\,\frac{\psi_n'(kr)}{kr}\,\frac{P_n^m(\cos\theta)}{\sin\theta}\,{\sin \atop \cos} m\phi\,\hat{\phi}$$

and

$$\psi_n(kr) = kr\, j_n(kr),$$

where $j_n(kr)$ is the spherical Bessel function of order n. $P_n^m(\cos\theta)$ is the Legendre function of degree n and order m as defined, for example, by Stratton (1941).

At the surface of the perfectly conducting sphere the scattered field $(\underline{E}^s, \underline{H}^s)$ satisfies the boundary condition

$$\hat{r} \times (\underline{E}^i + \underline{E}^s) = 0\ ,$$

and from the requirement that the scattered field represent an outgoing wave at infinity, we are led to write

$$\underline{E}^s = \sum_{n=1}^{\infty} \left(A_n \underline{M}^{(3)}_{o1n} + i B_n \underline{N}^{(3)}_{e1n} \right), \tag{3}$$

implying

$$\underline{H}^s = i\,Y \sum_{n=1}^{\infty} \left(A_n \underline{N}^{(3)}_{o1n} + i B_n \underline{M}^{(3)}_{e1n} \right) \ . \tag{4}$$

The $\underline{M}^{(3)}$ and $\underline{N}^{(3)}$ differ from the $\underline{M}^{(1)}$ and $\underline{N}^{(1)}$ in having $\psi_n(kr)$ replaced by

$$\zeta_n(kr) = kr\, h_n^{(2)}(kr)$$

where $h_n^{(2)}(kr)$ is the spherical Hankel function of the second kind. Application of the boundary condition at $r=a$ now gives

$$A_n = -i^n \frac{2n+1}{n(n+1)} \frac{\psi_n(ka)}{\zeta_n(ka)} , \qquad (5)$$

$$B_n = -i^n \frac{2n+1}{n(n+1)} \frac{\psi'_n(ka)}{\zeta'_n(ka)} , \qquad (6)$$

and by substitution of (5) and (6) into (3) and (4) the scattered field is then determined.

The total field is the sum of $(\underline{E}^i, \underline{H}^i)$ and $(\underline{E}^s, \underline{H}^s)$, and at the surface $r=a$ the only non-zero components are E_r, H_θ and H_ϕ. The last two are directly related to the components of the induced current $\underline{J}$ via the equation

$$\underline{J} = \hat{r} \times \underline{H} ,$$

so that

$$J_\theta = -H_\phi, \quad J_\phi = H_\theta ,$$

and if we define

$$H_\theta = Y \sin\phi \, T_1(\theta) \qquad (7)$$

$$H_\phi = Y \cos\phi \, T_2(\theta) , \qquad (8)$$

we have

$$T_1(\theta) = \frac{1}{ka} \sum_{n=1}^{\infty} i^{n+1} \frac{2n+1}{n(n+1)} \left\{ \frac{1}{\zeta'_n(ka)} \frac{P_n^1(\cos\theta)}{\sin\theta} + \frac{i}{\zeta_n(ka)} \frac{\partial}{\partial\theta} P_n^1(\cos\theta) \right\} \qquad (9)$$

$$T_2(\theta) = \frac{1}{ka} \sum_{n=1}^{\infty} i^{n+1} \frac{2n+1}{n(n+1)} \left\{ \frac{1}{\zeta'_n(ka)} \frac{\partial}{\partial\theta} P_n^1(\cos\theta) + \frac{i}{\zeta_n(ka)} \frac{P_n^1(\cos\theta)}{\sin\theta} \right\} . \qquad (10)$$

The interpretation of these in terms of creeping waves is discussed in Kazarinoff and Senior (1962).

In the far zone the scattered field behaves as an outgoing spherical wave whose properties can be obtained by replacing $\zeta_n(kr)$ and its derivative by the leading terms of their asymptotic expansions for large kr, viz.

$$\zeta_n'(kr) \sim -i\,\zeta_n(kr) \sim i^n\, e^{-ikr} \,. \tag{11}$$

Since $\underline{E}^s$ and $\underline{H}^s$ now satisfy the equation

$$\underline{H}^s = \hat{r} \times Y \underline{E}^s \,,$$

it is sufficient to confine our attention to the former, and following the notation* in Senior and Goodrich (1964), the components of the scattered electric vector are written as

$$E_\theta^s = i \cos\phi \, \frac{e^{-ikr}}{kr} \, S_1^s(\theta) \tag{12}$$

$$E_\phi^s = -i \sin\phi \, \frac{e^{-ikr}}{kr} \, S_2^s(\theta) \tag{13}$$

where

$$S_1^s(\theta) = \sum_{n=1}^{\infty} (-1)^n \frac{2n+1}{n(n+1)} \left\{ \frac{\psi_n'(ka)}{\zeta_n'(ka)} \frac{\partial}{\partial\theta} P_n^1(\cos\theta) - \frac{\psi_n(ka)}{\zeta_n(ka)} \frac{P_n^1(\cos\theta)}{\sin\theta} \right\} , \tag{14}$$

$$S_2^s(\theta) = \sum_{n=1}^{\infty} (-1)^n \frac{2n+1}{n(n+1)} \left\{ \frac{\psi_n'(ka)}{\zeta_n'(ka)} \frac{P_n^1(\cos\theta)}{\sin\theta} - \frac{\psi_n(ka)}{\zeta_n(ka)} \frac{\partial}{\partial\theta} P_n^1(\cos\theta) \right\} . \tag{15}$$

We note that

$$S_1^s(0) = S_2^s(0)$$

and

$$S_1^s(\pi) = -S_2^s(\pi) \,,$$

implying that, for back and forward scattering, the field has the same linear polarization as the incident field. In all other directions, however, the field is elliptically polarized and the component cross sections are

$$\sigma_\theta = \frac{\lambda^2}{\pi} \left| S_1^s(\theta) \right|^2 \cos^2\phi \,, \tag{16}$$

---

*Note the change in time convention.

$$\sigma_{\phi} = \frac{\lambda^2}{\pi} \left| S_2^s(\theta) \right|^2 \sin^2\phi \,. \tag{17}$$

The complete scattering cross section is, of course,

$$\sigma = \sigma_\theta + \sigma_\phi \,.$$

Let us now consider the separate but related problem of a perfectly conducting sphere with a narrow slot symmetrically placed with respect to the z direction (and hence, with respect to the incident field direction in the problem just discussed). The slot occupies the region $\theta_o - \delta/2 \leq \theta \leq \theta_o + \delta/2$ (see Figure 1) and its angular width δ is such that $ka\,\delta \ll 1$. Within the gap the tangential electric field is specified, and in view of our intention to regard the slot as semi-active by coupling the solution for this problem to the one already derived, the excitation must be chosen in accordance with the surface field behavior shown in equations (7) through (10). It is therefore assumed that for $\left|\theta - \theta_o\right| < \delta/2$

$$E_\theta = -\frac{v}{\delta a} \cos\phi \tag{18}$$

$$E_\phi = 0 \,, \tag{19}$$

corresponding to a constant (but asymmetrical) voltage $v\cos\phi$ across the gap. Over the rest of the sphere, E_θ and E_ϕ are both zero, as is appropriate to a perfectly conducting surface.

To determine the field $(\underline{E}^r, \underline{H}^r)$ radiated by the slot, we again postulate a field of the form shown in equations (3) and (4), but with A_n and B_n replaced by new constants C_n and D_n respectively, so that

$$\underline{E}^r = \sum_{n=1}^{\infty} \left(C_n \underline{M}_{o1n}^{(3)} + i D_n \underline{N}_{e1n}^{(3)} \right) \,, \tag{20}$$

$$\underline{H}^r = i Y \sum_{n=1}^{\infty} \left(C_n \underline{N}_{o1n}^{(3)} + i D_n \underline{M}_{e1n}^{(3)} \right) \,. \tag{21}$$

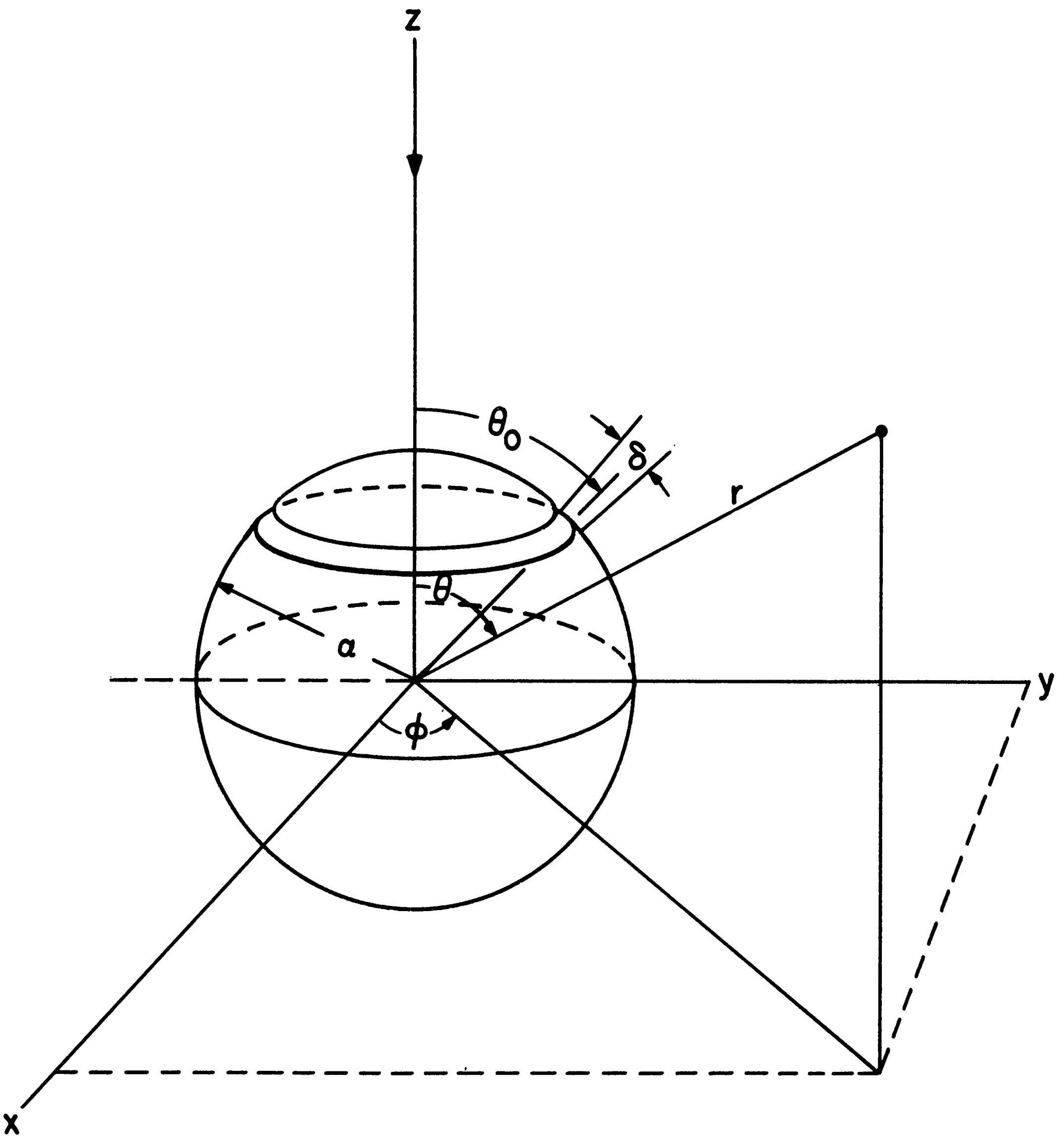

FIGURE 1: SPHERE GEOMETRY

When these are substituted into the boundary conditions at $r = a$, we obtain

$$\sum_{n=1}^{\infty} \left\{ C_n \zeta_n(ka) \frac{P_n^1(\cos\theta)}{\sin\theta} + i D_n \zeta_n'(ka) \frac{\partial}{\partial\theta} P_n^1(\cos\theta) \right\} = -\frac{kv}{\delta}, \quad \left|\theta - \theta_o\right| < \frac{\delta}{2}$$

$$= 0, \qquad \text{otherwise,} \tag{22}$$

from the θ component, and

$$\sum_{n=1}^{\infty} \left\{ C_n \zeta_n(ka) \frac{\partial}{\partial\theta} P_n^1(\cos\theta) + i D_n \zeta_n'(ka) \frac{P_n^1(\cos\theta)}{\sin\theta} \right\} = 0, \quad \text{all } \theta, \tag{23}$$

from the ϕ component. Moreover, from Bailin and Silver (1956)

$$\int_0^{\pi} \left\{ P_n^1(\cos\theta) \frac{\partial}{\partial\theta} P_m^1(\cos\theta) + P_m^1(\cos\theta) \frac{\partial}{\partial\theta} P_n^1(\cos\theta) \right\} d\theta = 0$$

and

$$\int_0^{\pi} \left\{ \frac{\partial}{\partial\theta} P_n^1(\cos\theta) \frac{\partial}{\partial\theta} P_m^1(\cos\theta) + \frac{1}{\sin^2\theta} P_n^1(\cos\theta) P_m^1(\cos\theta) \right\} \sin\theta \, d\theta = \Lambda_{nm}$$

where

$$\Lambda_{nm} = \begin{cases} 0 & n \neq m \\ \dfrac{2n^2(n+1)^2}{2n+1} & n = m \end{cases},$$

and hence, by application of these relations to (22) and (23),

$$C_n = -\frac{kv}{\zeta_n(ka)} \frac{2n+1}{2n^2(n+1)^2} \frac{1}{\delta} \int_{\theta_o - \delta/2}^{\theta_o + \delta/2} P_n^1(\cos\theta) d\theta$$

$$= \frac{kv}{\zeta_n(ka)} \frac{2n+1}{2n^2(n+1)^2} \frac{P_n(+) - P_n(-)}{\delta} \tag{24}$$

and

$$D_n = i \frac{kv}{\zeta_n'(ka)} \frac{2n+1}{2n^2(n+1)^2} \frac{1}{\delta} \int_{\theta_o-\delta/2}^{\theta_o+\delta/2} \sin\theta \frac{\partial}{\partial\theta} P_n^1(\cos\theta)d\theta$$

$$\simeq i \frac{kv\sin\theta_o}{\zeta_n'(ka)} \frac{2n+1}{2n^2(n+1)^2} \frac{P_n^1(+) - P_n^1(-)}{\delta} \tag{25}$$

where, for brevity, we have written

$$P_n^m(\pm) = P_n^m\left(\cos\left\{\theta_o \pm \frac{\delta}{2}\right\}\right) .$$

In evaluating D_n it was assumed that the variation of $\sin\theta$ over the slot can be neglected, and consequently the position of the slot is now limited by the condition

$$\epsilon \leq \theta_o \leq \pi - \epsilon$$

with $\epsilon >> \delta$. It is also observed that in the limit $\delta \rightarrow 0$

$$\frac{P_n(+) - P_n(-)}{\delta} \longrightarrow -P_n^1(\cos\theta_o)$$

and

$$\frac{P_n^1(+) - P_n^1(-)}{\delta} \longrightarrow \frac{\partial}{\partial\theta_o} P_n^1(\cos\theta_o) .$$

The expressions for the components of the radiated field follow from equations (20) and (21) on inserting the above formulae for C_n and D_n. Two particular cases are of interest. On the surface $r = a$ we have, analogously to (7) and (8),

$$H_\theta^r = Yv\sin\phi\, T_1^r(\theta) \tag{26}$$

and

$$H_\phi^r = Yv\cos\phi\, T_2^r(\theta), \tag{27}$$

where

$$T_1^r(\theta) = \frac{i}{2a} \sum_{n=1}^{\infty} \frac{2n+1}{n^2(n+1)^2} \left\{ \frac{\zeta_n(ka)}{\zeta_n'(ka)} \frac{\sin\theta_o}{\sin\theta} \left(\frac{P_n^1(+) - P_n^1(-)}{\delta} \right) P_n^1(\cos\theta) \right.$$

$$\left. + \frac{\zeta_n'(ka)}{\zeta_n(ka)} \left(\frac{P_n(+) - P_n(-)}{\delta} \right) \frac{\partial}{\partial\theta} P_n^1(\cos\theta) \right\}, \tag{28}$$

$$T_2^r(\theta) = \frac{i}{2a} \sum_{n=1}^{\infty} \frac{2n+1}{n^2(n+1)^2} \left\{ \frac{\zeta_n(ka)}{\zeta_n'(ka)} \sin\theta_o \left(\frac{P_n^1(+) - P_n^1(-)}{\delta} \right) \frac{\partial}{\partial\theta} P_n^1(\cos\theta) \right.$$

$$\left. + \frac{\zeta_n'(ka)}{\zeta_n(ka)} \frac{1}{\sin\theta} \left(\frac{P_n(+) - P_n(-)}{\delta} \right) P_n^1(\cos\theta) \right\} \tag{29}$$

The rates at which the above series converge are functions of δ and θ as well as ka. If $\delta \neq 0$, the series for $T_2^r(\theta)$ converges for all θ, but for $T_1^r(\theta)$ the convergence decreases rapidly as θ approaches $\theta_o \pm \delta/2$, and in the limit the series actually diverges. This behavior can be attributed to the step discontinuity in the surface field introduced by (18). The two series also diverge if $\delta = 0$, and to effect a numerical evaluation it is therefore necessary to keep δ non-zero and to retain a number N of terms which is, in fact, inversely proportional to δ.

In the far zone, on the other hand, the expressions for the field components are convergent even for $\delta = 0$, corresponding to an infinitesimal slot across which the voltage $v\cos\phi$ is applied. For simplicity we shall therefore proceed directly to the limit, in which case

$$E_\theta^r = iv\cos\phi \, \frac{e^{-ikr}}{kr} S_1^r(\theta) , \tag{30}$$

$$E_\phi^r = -iv\sin\phi \, \frac{e^{-ikr}}{kr} S_2^r(\theta) \tag{31}$$

(cf equations (12) and (13)) with

$$S_1^r(\theta) = \frac{k}{2}\sin\theta_o \sum_{n=1}^{\infty} i^{n+1} \frac{2n+1}{n^2(n+1)^2}\left\{\frac{1}{\zeta_n'(ka)} \frac{\partial}{\partial\theta} P_n^1(\cos\theta) \frac{\partial}{\partial\theta_o} P_n^1(\cos\theta_o)\right.$$

$$\left. + \frac{i}{\zeta_n(ka)} \frac{P_n^1(\cos\theta)}{\sin\theta} \frac{P_n^1(\cos\theta_o)}{\sin\theta_o}\right\}, \tag{32}$$

$$S_2^r(\theta) = \frac{k}{2}\sin\theta_o \sum_{n=1}^{\infty} i^{n+1} \frac{2n+1}{n^2(n+1)^2}\left\{\frac{1}{\zeta_n'(ka)} \frac{P_n^1(\cos\theta)}{\sin\theta} \frac{\partial}{\partial\theta_o} P_n^1(\cos\theta_o)\right.$$

$$\left. + \frac{i}{\zeta_n(ka)} \frac{\partial}{\partial\theta} P_n^1(\cos\theta) \frac{P_n^1(\cos\theta_o)}{\sin\theta_o}\right\}, \tag{33}$$

and from these the components of the magnetic vector can be obtained as before.

The final problem to be considered is a combination of the preceding two in which the plane wave given in equations (1) and (2) is incident on the slotted sphere. If it is assumed that the same voltage is excited across the gap, the expressions for the resulting fields can be found by superposition of those associated with each individual problem. We therefore have

$$\underline{E} = \underline{E}^i + \underline{E}^s + \underline{E}^r \tag{34}$$

and

$$\underline{H} = \underline{H}^i + \underline{H}^s + \underline{H}^r , \tag{35}$$

where $(\underline{E}^s, \underline{H}^s)$ and $(\underline{E}^r, \underline{H}^r)$ are as given above. In particular, in the far zone, the components of the total scattered electric field are

$$E_\theta = i\cos\phi \frac{e^{-ikr}}{kr} S_1(\theta) , \tag{36}$$

$$E_\phi = -i\sin\phi \frac{e^{-ikr}}{kr} S_2(\theta) \tag{37}$$

with

$$S_1(\theta) = S_1^s(\theta) + vS_1^r(\theta) , \tag{38}$$

$$S_2(\theta) = S_2^s(\theta) + v\,S_2^r(\theta) \quad . \tag{39}$$

The expressions for S_1^r and S_2^r are, of course, independent of v, and if this voltage is induced by a loading applied to the slot (using, for example, a cavity at its back), the voltage can be related to the loading admittance. The derivation of this equation is our next task.

III
RADIATION AND LOADING ADMITTANCES

In antenna theory it is customary to define the admittance of a slot as the ratio of the current flowing away from the gap to the applied voltage, where the latter is the line integral of the electric field across the gap. In the present problem, however, the total instantaneous current is zero, due to the $\cos\phi$ variation of the slot excitation; some other definition of admittance is therefore necessary, and it is natural to introduce the concept of admittance density, where this is the ratio of the current density to the applied voltage at a point specified by the azimuthal variable ϕ.

The implications of such a definition can be seen by considering the radiation admittance of the slot in the second of the three problems discussed in Section II. Since the current flowing from the slot is

$$J_\theta = -H^r_\phi \ ,$$

the radiation admittance density is

$$y_r = \frac{J_\theta}{v\cos\phi}$$
$$= -Y\, T^r_2(\theta) \ ,$$

and hence the (total) radiation admittance is

$$Y_r = \int_0^{2\pi} y_r \, a \sin\theta_o \, d\phi$$
$$= -2\pi\, a \sin\theta_o \, Y\, T^r_2(\theta) \ . \tag{40}$$

As written above, however, Y_r does not provide a unique specification of the admittance. Since the slot width δ must be non-zero in order to compute $T^r_2(\theta)$

it would be possible to give θ any value between $\theta_o - \delta/2$ and $\theta_o + \delta/2$, and though the numerical effect on Y_r may be insignificant under most practical circumstances, it is undesirable that the expression for Y_r should have that degree of arbitrariness.

In an attempt to overcome the disadvantage, we note that an alternative, but equally acceptable, definition of admittance is twice the ratio of the complex power flow across the aperture to the square of the voltage, and for the case in which the voltage is a function of position along the slot, the concept of admittance density is once again appropriate. The complex power radiated per unit length of the slot is

$$w = \int_{\theta_o - \delta/2}^{\theta_o + \delta/2} \frac{1}{2}(\underline{E}^r \times \underline{\tilde{H}}^r) \cdot \hat{r}\, a d\theta$$

$$= -\frac{1}{2}\,\frac{v\cos\phi}{\delta} \int_{\theta_o - \delta/2}^{\theta_o + \delta/2} \tilde{H}^r_\phi \, d\theta \ ,$$

where $\sim$ denotes the complex conjugate. The radiation admittance density is therefore

$$y_r = \frac{2\tilde{w}}{(v\cos\phi)^2}$$

$$= \frac{-1}{\delta v \cos\phi} \int_{\theta_o - \delta/2}^{\theta_o + \delta/2} H^r_\phi \, d\theta \ , \qquad (41)$$

and using the expression for H_ϕ given in equation (27), together with the evaluation of the Legendre function integrals employed in the determination of C_n and D_n, we have

$$y_r = iY\frac{\sin\theta_o}{2a} \sum_{n=1}^{\infty} \frac{2n+1}{n^2(n+1)^2} \left\{ \frac{\zeta_n'(ka)}{\zeta_n(ka)} \left(\frac{P_n(+) - P_n(-)}{\delta \sin\theta_o} \right)^2 - \frac{\zeta_n(ka)}{\zeta_n'(ka)} \left(\frac{P_n^1(+) - P_n^1(-)}{\delta} \right)^2 \right\}$$

Hence

$$Y_r = i\,Y\pi \sin^2\theta_o \sum_{n=1}^{\infty} \frac{2n+1}{n^2(n+1)^2} \left\{ \frac{\zeta_n'(ka)}{\zeta_n(ka)} \left(\frac{P_n(+) - P_n(-)}{\delta \sin\theta_o} \right)^2 - \frac{\zeta_n(ka)}{\zeta_n'(ka)} \left(\frac{P_n^1(+) - P_n^1(-)}{\delta} \right)^2 \right\} \tag{42}$$

and in contrast to the expression for Y_r originally derived, this new result has no ambiguity. The computation of equation (42) is discussed in Section IV.

Let us now apply this same technique to the determination of the loading admittance in the case of a semi-active slot (third problem in Section II). As before, the complex power per unit length of the slot is obtained by integrating the Poynting vector, and for power entering into the slot

$$w = -\int_{\theta_o-\delta/2}^{\theta_o+\delta/2} \frac{1}{2}(\underline{E} \times \underline{\tilde{H}}) \cdot \hat{r}\, d\theta$$

where $(\underline{E}, \underline{H})$ are as given in equations (34) and (35). Thus

$$w = \frac{1}{2}\,\frac{v \cos\phi}{\delta} \int_{\theta_o-\delta/2}^{\theta_o+\delta/2} \tilde{H}_\phi\, d\theta$$

and the slot admittance density is

$$y_\ell = \frac{1}{\delta v \cos\phi} \int_{\theta_o-\delta/2}^{\theta_o+\delta/2} (H_\phi^i + H_\phi^s + H_\phi^r)\, d\theta \ ,$$

which can be written as

$$y_\ell = -y_r + \frac{Y}{\delta v} \int_{\theta_o-\delta/2}^{\theta_o+\delta/2} T_2(\theta)\, d\theta \tag{43}$$

by using equations (41), (8), and (10). For δ sufficiently small, the variation of $T_2(\theta)$ across the slot can be neglected, giving

$$y_\ell = -y_r + \frac{Y}{v} T_2(\theta_o) \ ,$$

and the total loading admittance of the slot is therefore

$$Y_\ell = -Y_r + \frac{Y}{v} 2\pi a \sin\theta_o T_2(\theta_o) \,, \tag{44}$$

where Y_r and $T_2(\theta_o)$ are as shown in equations (42) and (10) respectively.

Y_ℓ is the significant parameter for control of the scattering behavior. Solving for v,

$$v = \frac{Y}{Y_\ell + Y_r} 2\pi a \sin\theta_o T_2(\theta_o) \,, \tag{45}$$

which can be substituted into the expressions for $S_1^r(\theta)$ and $S_2^r(\theta)$ to give the total scattering amplitudes

$$S_1(\theta) = S_1^s(\theta) + \frac{Y}{Y_\ell + Y_r} 2\pi a \sin\theta_o T_2(\theta_o) S_1^r(\theta) \tag{46}$$

$$S_2(\theta) = S_2^s(\theta) + \frac{Y}{Y_\ell + Y_r} 2\pi a \sin\theta_o T_2(\theta_o) S_2^r(\theta) \tag{47}$$

(see equations (38) and (39)). The right hand sides of (46) and (47) are functions only of ka, δ, θ_o and θ, and in particular, are independent of v.

To make the scattering amplitude $S_1(\theta)$ zero in the direction $\theta = \theta'$, the loading required is

$$Y_\ell = -Y_r - Y\, 2\pi a \sin\theta_o T_2(\theta_o) \frac{S_1^r(\theta')}{S_1^s(\theta')} \,. \tag{48}$$

This differs from the loading necessary to make $S_2(\theta)$ zero for $\theta = \theta'$ unless

$$\frac{S_1^r(\theta')}{S_1^s(\theta')} = \frac{S_2^r(\theta')}{S_2^s(\theta')} \,, \tag{49}$$

and thus in general the complete scattering cross section $\sigma = \sigma_\theta + \sigma_\phi$ cannot be reduced to zero with a loading of the form discussed here. This does not, however, rule out the possibility of significant reductions in σ by suitable choice of Y_r. Moreover, in many cases of bistatic scattering only $S_1(\theta)$ or $S_2(\theta)$ is of interest, and a zero (component) cross section can then be achieved.

The obvious exceptions to the above are back and forward scattering. The back scattering direction is $\theta = 0$, and here

$$\left[\frac{P_n^1(\cos\theta)}{\sin\theta}\right]_{\theta=0} = \frac{n(n+1)}{2} = \left[\frac{\partial}{\partial\theta} P_n^1(\cos\theta)\right]_{\theta=0} ,$$

from which we have

$$S_1^s(0) = S_2^s(0) ,$$

$$S_1^r(0) = S_2^r(0) .$$

Furthermore,

$$S_1^r(0) = \frac{k}{4} ka \sin\theta_o T_2(\theta_o) \tag{50}$$

and hence the loading for zero $S_1(0)$ and $S_2(0)$ is

$$\begin{aligned} Y_\ell &= -Y_r - Y\frac{\pi}{2}\left\{ka \sin\theta_o T_2(\theta_o)\right\}^2 \left\{S_1^s(0)\right\}^{-1} \\ &= -Y_r - Y\pi\left\{ka \sin\theta_o T_2(\theta_o)\right\}^2 \left\{\sum_{n=1}^{\infty}(-1)^n(2n+1)\left(\frac{\psi_n'(ka)}{\zeta'(ka)} - \frac{\psi_n(ka)}{\zeta_n(ka)}\right)\right\}^{-1} . \end{aligned} \tag{51}$$

This corresponds to either an active or passive load depending on the values of ka and θ_o. Similarly, for the forward scattering direction $(\theta = \pi)$

$$\left[\frac{P_n^1(\cos\theta)}{\sin\theta}\right]_{\theta=\pi} = (-1)^{n+1} \frac{n(n+1)}{2} = -\left[\frac{\partial}{\partial\theta} P_n^1(\cos\theta)\right]_{\theta=\pi} ,$$

so that

$$S_1^s(\pi) = -S_2^s(\pi) ,$$

$$S_1^r(\pi) = -S_2^r(\pi) ,$$

and these also satisfy the conditions (49). Moreover,

$$S_1^r(\pi) = -\frac{k}{4}\sin\theta_o \sum_{n=1}^{\infty} (-i)^{n+1} \frac{2n+1}{n(n+1)} \left\{ \frac{1}{\zeta_n'(ka)} \frac{\partial}{\partial\theta_o} P_n^1(\cos\theta_o) - \frac{i}{\zeta_n(ka)} \frac{P_n^1(\cos\theta_o)}{\sin\theta_o} \right\} \tag{52}$$

$$= \frac{k}{4}\, ka \sin\theta_o T_2(\pi-\theta_o) \ ,$$

and consequently for zero $S_1(\pi)$ and $S_2(\pi)$

$$Y_\ell = -Y_r - Y\frac{\pi}{2}(ka\sin\theta_o)^2\, T_2(\theta_o)T_2(\pi-\theta_o) \left\{ S_1^s(\pi) \right\}^{-1}$$

$$= -Y_r - Y\pi(ka\sin\theta_o)^2\, T_2(\theta_o)T_2(\pi-\theta_o) \left\{ \sum_{n=1}^{\infty}(2n+1)\left(\frac{\psi_n'(ka)}{\zeta_n'(ka)} - \frac{\psi_n(ka)}{\zeta_n(ka)} \right) \right\}^{-1} . \tag{53}$$

The fact that for a passive object zero scattering in the forward direction implies zero total scattering and zero absorption (Schiff, 1954) indicates that the above loading corresponds to an active slot for all ka and θ_o.

If $\theta \neq \pi$ the characteristics of the loading admittance for zero $S_1(\theta)$ or $S_2(\theta)$ can in general be determined only by numerical computation of the functions involved. An exception is the case of small ka. Using the small argument expansions for $\psi_n(ka)$, $\zeta_n(ka)$ and their derivatives, it is found that the admittance necessary to make $S_1(\theta)$ zero is

$$Y_\ell^{(1)} = Y\frac{\pi}{ka}\left\{ i\,\gamma_{01} + \gamma_{11}ka + O(\overline{ka}^2) \right\} \tag{54}$$

(see equation (48)), where

$$\gamma_{01} = -\frac{9}{4}\,\frac{\sin^2\theta_o}{1+2\cos\theta} + \sum_{n=1}^{\infty} \frac{2n+1}{n(n+1)^2}\left(\frac{P_n(+) - P_n(-)}{\delta} \right)^2 ,$$

$$\gamma_{11} = \frac{7}{2}\,\frac{1+\cos\theta}{1+2\cos\theta}\,\sin^2\theta_o\cos\theta_o \ ;$$

similarly, to make $S_2(\theta)$ zero

$$Y_\ell^{(2)} = Y\frac{\pi}{ka}\left\{i\gamma_{02}+\gamma_{12}ka+O(\overline{ka}^2)\right\} \tag{55}$$

where

$$\gamma_{02} = -\frac{9}{4}\,\frac{\sin^2\theta_o\cos\theta}{2+\cos\theta}+\sum_{n=1}^{\infty}\frac{2n+1}{n(n+1)^2}\left(\frac{P_n(+)-P_n(-)}{\delta}\right)^2 ,$$

$$\gamma_{12} = \frac{1}{2}\,\frac{(1+\cos\theta)\,(2+5\cos\theta)}{2+\cos\theta}\,\sin^2\theta_o\cos\theta_o \;.$$

As expected, the two admittances are identical for $\theta = 0$ and π, but to the order shown the expansions give no applicable information about the real part of the admittance in the forward direction. For $\theta \neq \pi$, however, the dominant contributions to $\mathrm{Re}.Y_\ell$ are provided by γ_{11} and γ_{12}, and these show a significant change of character as θ passes through a critical value. Thus, for example, $\mathrm{Re}.Y_\ell^{(1)}$ has the same sign as $\frac{\cos\theta_o}{1+2\cos\theta}$, corresponding to an active or passive load according as this ratio is negative or positive respectively, and to reduce the back scattering cross section of a small sphere to zero with a passive load it is therefore necessary that $\theta_o \leq \pi/2$

IV
COMPUTED RESULTS

The six functions $S_1^s(\theta)$, $S_2^s(\theta)$, $S_1^r(\theta)$, $S_2^r(\theta)$, $T_2(\theta_o)$ and Y_r involved in the expressions for $S_1(\theta)$ and $S_2(\theta)$ (see equations (46) and (47)) were programmed for calculation on the University of Michigan IBM 7090 computer, and because of the practical significance which each of these functions has, it is of interest to examine their individual values before discussing the loading necessary for particular cross section modifications. Except in the case of Y_r, all of the computations were straightforward. The number N of terms retained in any one series was essentially a machine variable, and was the largest possible consistent with the machine capacity not being exceeded in any of the subsidiary calculations associated with that term. In practice it turned out that N was of order 5 + 4ka, and to judge from the results obtained using a somewhat smaller number of terms, it would appear that this was sufficient for four digit accuracy.

$S_1^s(\theta)$ and $S_2^s(\theta)$ are the complex far field amplitudes for the solid (unloaded) sphere, and the corresponding component scattering cross sections are given by equations (16) and (17). The case of back scattering $(\theta = 0)$ is of most concern. The two functions are then equal, and since adequate tabulations are available in the literature (Bechtel, 1962), no further computations were performed. For reference purposes, however, the back scattering cross section

$$\sigma(0) = \frac{\lambda^2}{\pi} \left| S_1^s(0) \right|^2 \tag{56}$$

normalized to the physical optics value πa^2, is plotted as a function of ka for $0 \leq ka \leq 10$ in Figure 2.

$T_2(\theta)$ is proportional to that component of the current on the solid sphere which, in the shadow region, gives rise to the major creeping wave (Kazarinoff and Senior, 1962). The component is also normal to the slot and, as such, will excite the slot and be altered by the presence of an annular perturbation at the surface. To illustrate the variation as a function of θ, $T_2(\theta)$ has been computed for $0 \leq 0 \leq 180^o$

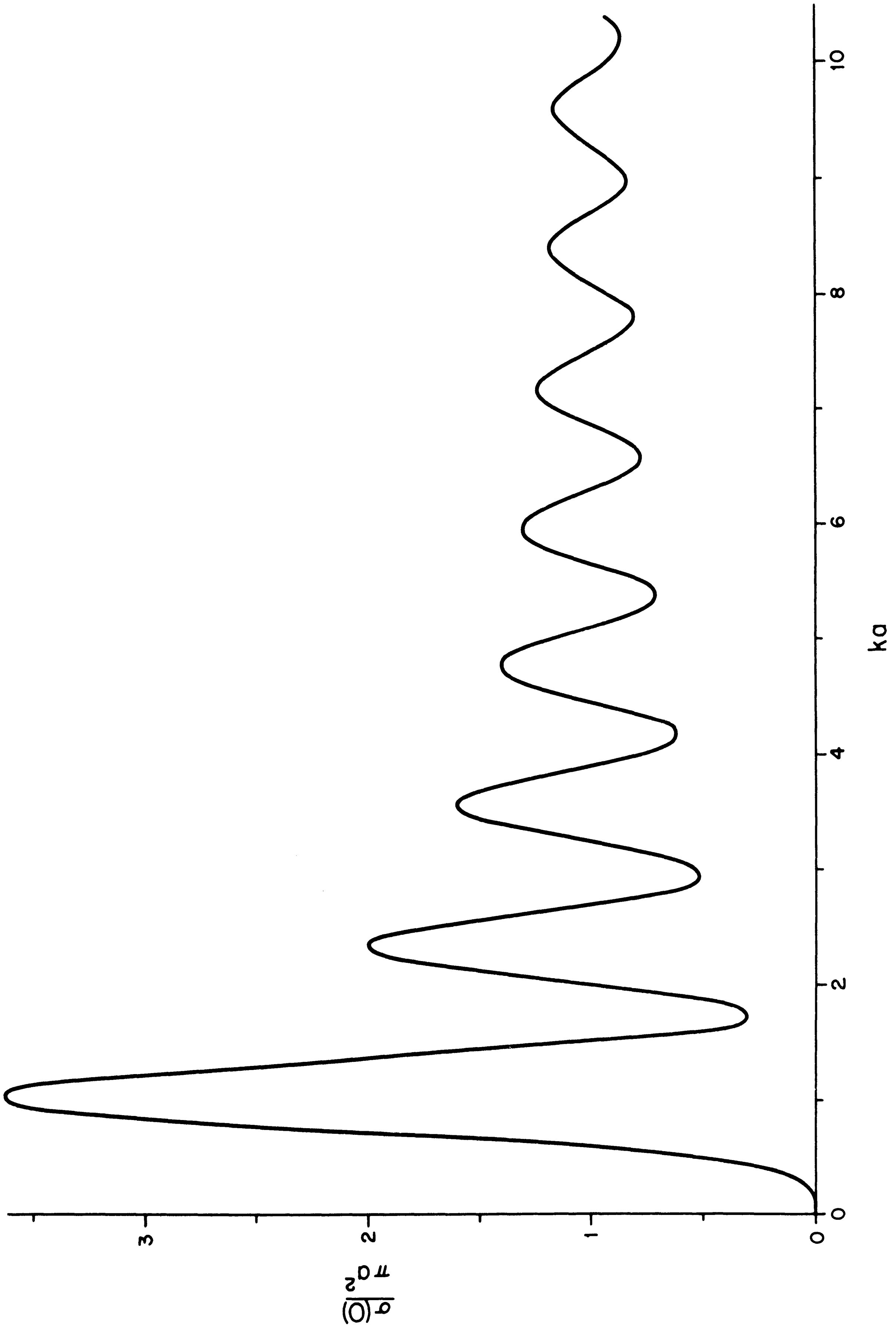

FIG. 2: NORMALIZED BACK SCATTERING CROSS SECTION OF UNLOADED SPHERE.

in increments of 5^{o} with ka = 4.28, and the results are shown in Figure 3. The oscillatory behavior within the shadow is apparent. Computations were also made for ka = 0(0.1)10.0 with $\theta = 60^{o}$, 90^{o} and 120^{o}, and the moduli are presented in Figure 4. On passing from the lit region to the shadow there is a fairly systematic reduction in magnitude which is most evident for the larger values of ka. As ka → 0, however, the amplitude tends to 1.5 regardless of θ.

In the back scattering direction $S_1^r(\theta)$ and $S_2^r(\theta)$ are equal and proportional to $T_2(\theta_o)$ (see equation (50)), so that separate computation of these functions is not necessary as long as $\theta = 0$. For other directions, however, the procedure is quite straightforward and is mentioned briefly later on.

The evaluation of the series for the radiation admittance Y_r is complicated by the slow convergence of its imaginary part for all non-zero δ. This is a consequence of the local capacitance in the vicinity of the gap and, indeed, in the limit as the gap width tends to zero, the series for the imaginary part fails to converge. In contrast, the series for the real part is rapidly convergent even for $\delta = 0$.

To facilitate the computations, the first N terms of the series are treated exactly and the subsequent terms are replaced by their asymptotic forms for large n (Plonus, to be published). Since

$$\frac{\zeta_n(ka)}{\zeta_n'(ka)} \sim \frac{n}{ka} \tag{57}$$

for $n \gg ka$, and

$$P_n(\cos\theta) \sim \sqrt{\frac{2}{n\pi\sin\theta}}\cos\left\{(n+\frac{1}{2})\theta - \frac{\pi}{4}\right\}$$

$$P_n^1(\cos\theta) \sim \sqrt{\frac{2n}{\pi\sin\theta}}\cos\left\{(n+\frac{1}{2})\theta + \frac{\pi}{4}\right\}$$

for $n \gg \operatorname{cosec}\theta$, substitution of these expressions into the higher order terms of (42) gives

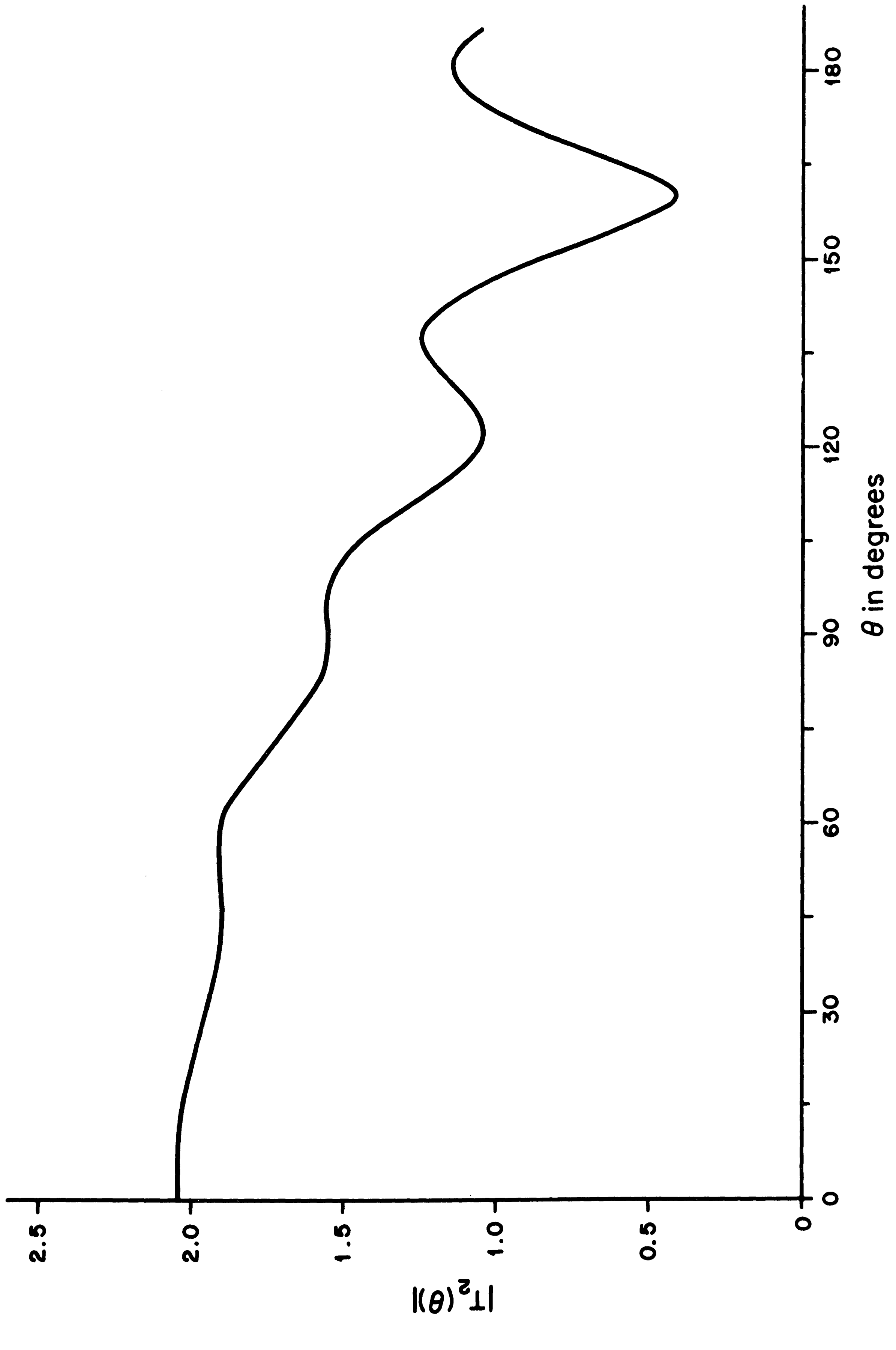

FIG. 3: AMPLITUDE OF SURFACE FIELD COMPONENT $T_2(\theta)$ FOR ka=4.28.

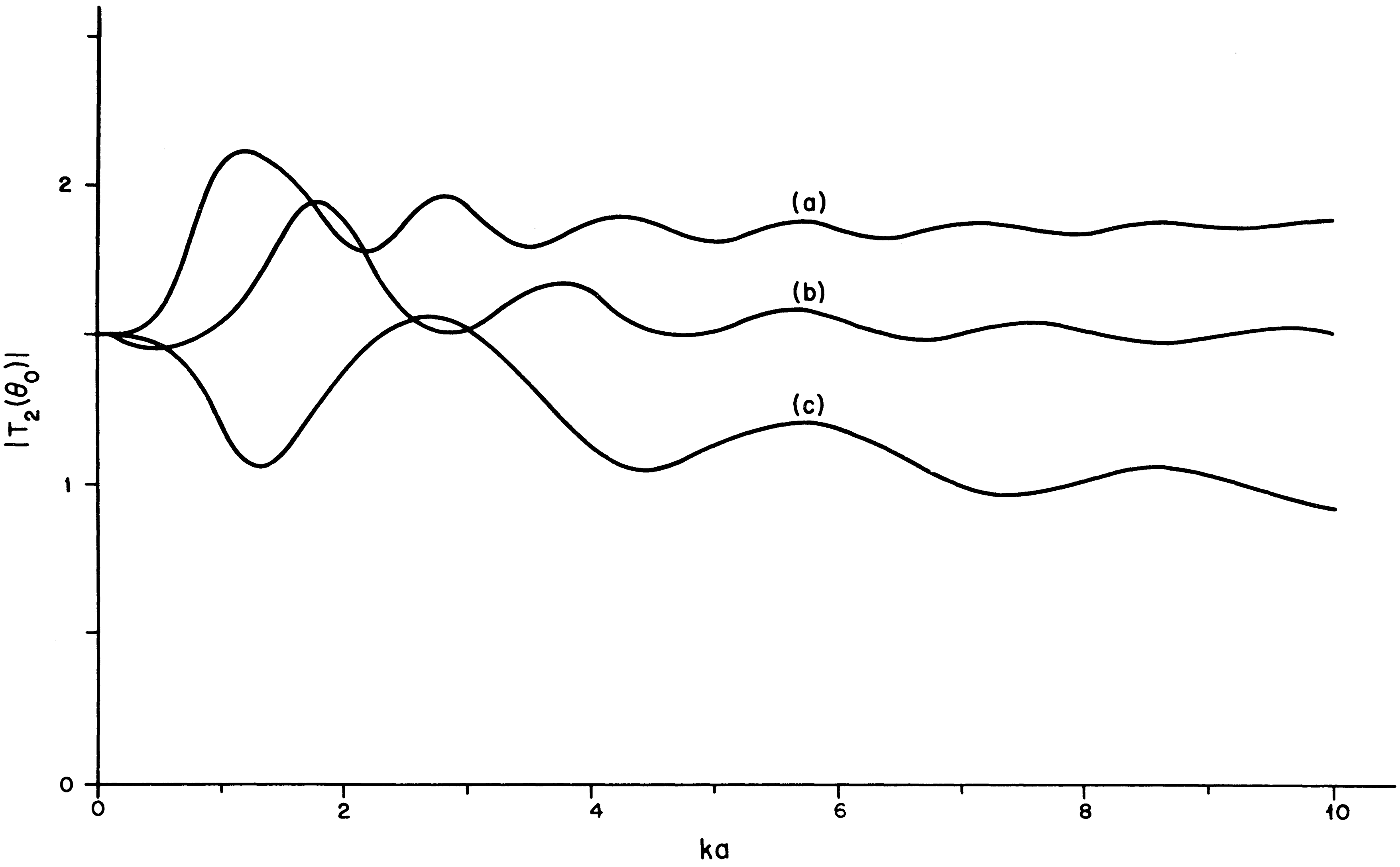

FIG. 4: AMPLITUDE OF SURFACE FIELD COMPONENT $T_2(\theta_o)$ FOR (a) $\theta_o = 60^o$, (b) $\theta_o = 90^o$ and (c) $\theta_o = 120^o$.

$$\frac{Y_r}{Y} \simeq i\pi \sin^2\theta_o \sum_{n=1}^{N} \frac{2n+1}{n^2(n+1)^2} \left\{ \frac{\zeta_n'(ka)}{\zeta_n(ka)} \left(\frac{P_n(+) - P_n(-)}{\delta \sin\theta_o} \right)^2 - \frac{\zeta_n(ka)}{\zeta_n'(ka)} \left(\frac{P_n^1(+) - P_n^1(-)}{\delta} \right)^2 \right\}$$

$$+ i \sum_{n=N+1}^{\infty} \frac{2n+1}{n^2(n+1)^2} \left(\frac{\sin\frac{n\delta}{2}}{\frac{n\delta}{2}} \right)^2 \left[ka \sin\theta_o \left\{ 1 + \sin(2n+1)\theta_o \right\} - \frac{1}{ka \sin\theta_o} \left\{ 1 - \sin(2n+1)\theta_o \right\} \right]. \tag{58}$$

In all of the computations, N was given the largest value consistent with machine capacity, and 1000 terms were retained in the second series. This last is certainly more than sufficient for our purposes, and the only possible source of error then lies in the use of asymptotic formulae. To get some feeling for the probable magnitude of these errors, Y_r/Y was computed for $ka = 5.0$, $\delta = 0.0392$ and $\theta_o = 90^o$ using four different values for the upper limit of the summation variable in the first series, and the results are summarized below:

$N = 10$, $\quad Y_r/Y = 15.255 + i\,29.686$,

$N = 15$, $\quad Y_r/Y = 15.255 + i\,30.385$,

$N = 20$, $\quad Y_r/Y = 15.255 + i\,30.676$,

$N = 24$, $\quad Y_r/Y = 15.255 + i\,30.748$.

($N = 24$ is the maximum attainable by the machine for $ka = 5.0$). The rapid convergence of the series for Re. Y_r is reflected in the constancy of the real parts above, and if the trend of the imaginary parts remains the same as N is increased still further, the computed magnitude of Im. Y_r with $N = 24$ should be within one per cent of the correct value.

Since the expression for Y_r is symmetrical about $\theta_o = 90^o$, it is sufficient to restrict attention to $\theta_o \leq 90^o$, and the values that were chosen for computation were $\theta_o = 60^o$ and 90^o with $\delta = 0.0392$ (approximately 2.25^o). The real and imaginary parts of Y_r/Y for the two cases are plotted as functions of ka, $0 \leq ka \leq 10$, in Figures 5 and 6 respectively, and from these it would appear that a change of slot position does not affect the general character of the curves. The real parts are zero for $ka = 0$, and rise through positive values with a small but regular

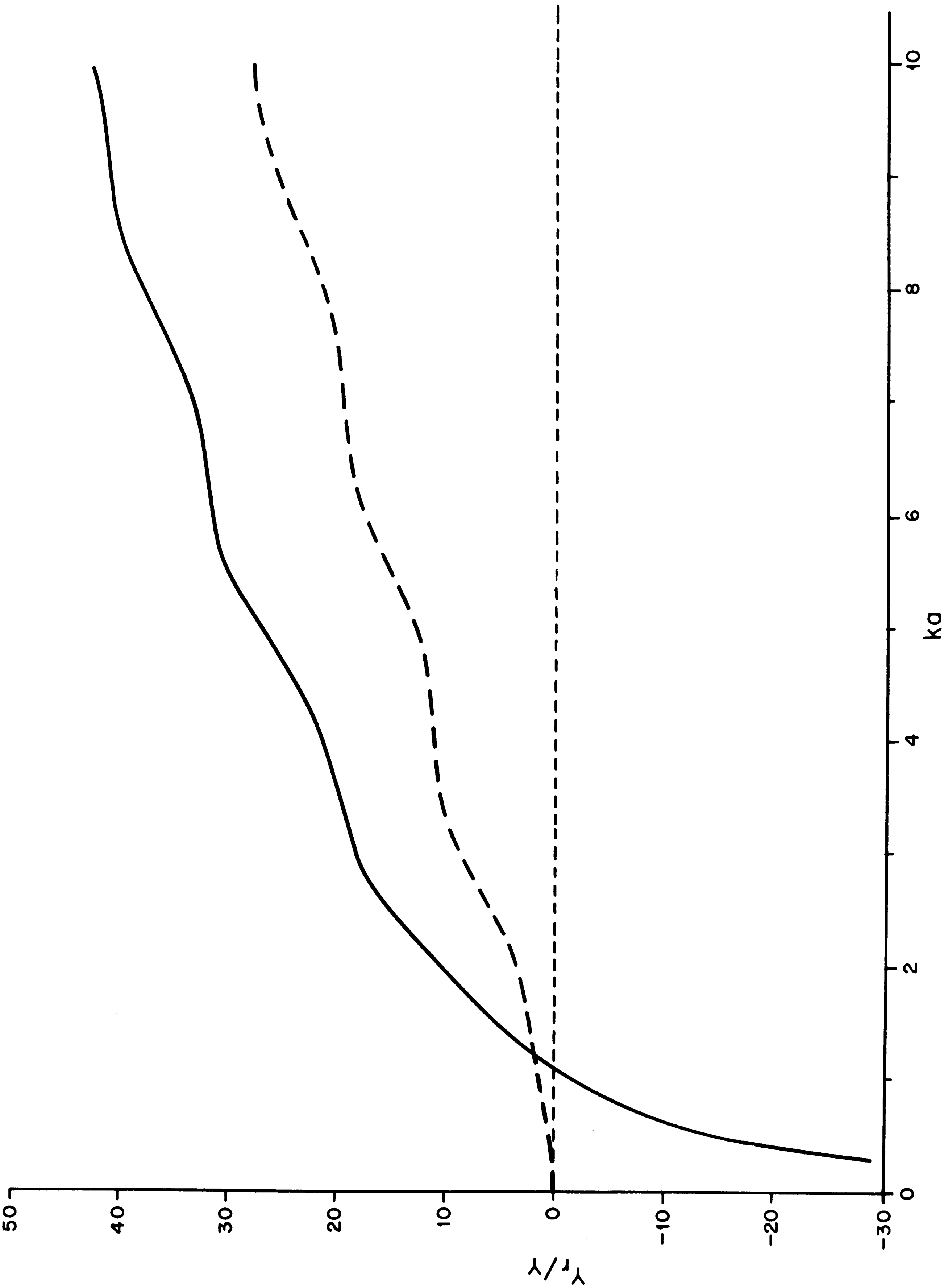

FIG. 5: REAL (---) AND IMAGINARY (—) PARTS OF NORMALIZED RADIATION ADMITTANCE FOR $\theta_o = 60^o$ AND $\delta = 0.0392$.

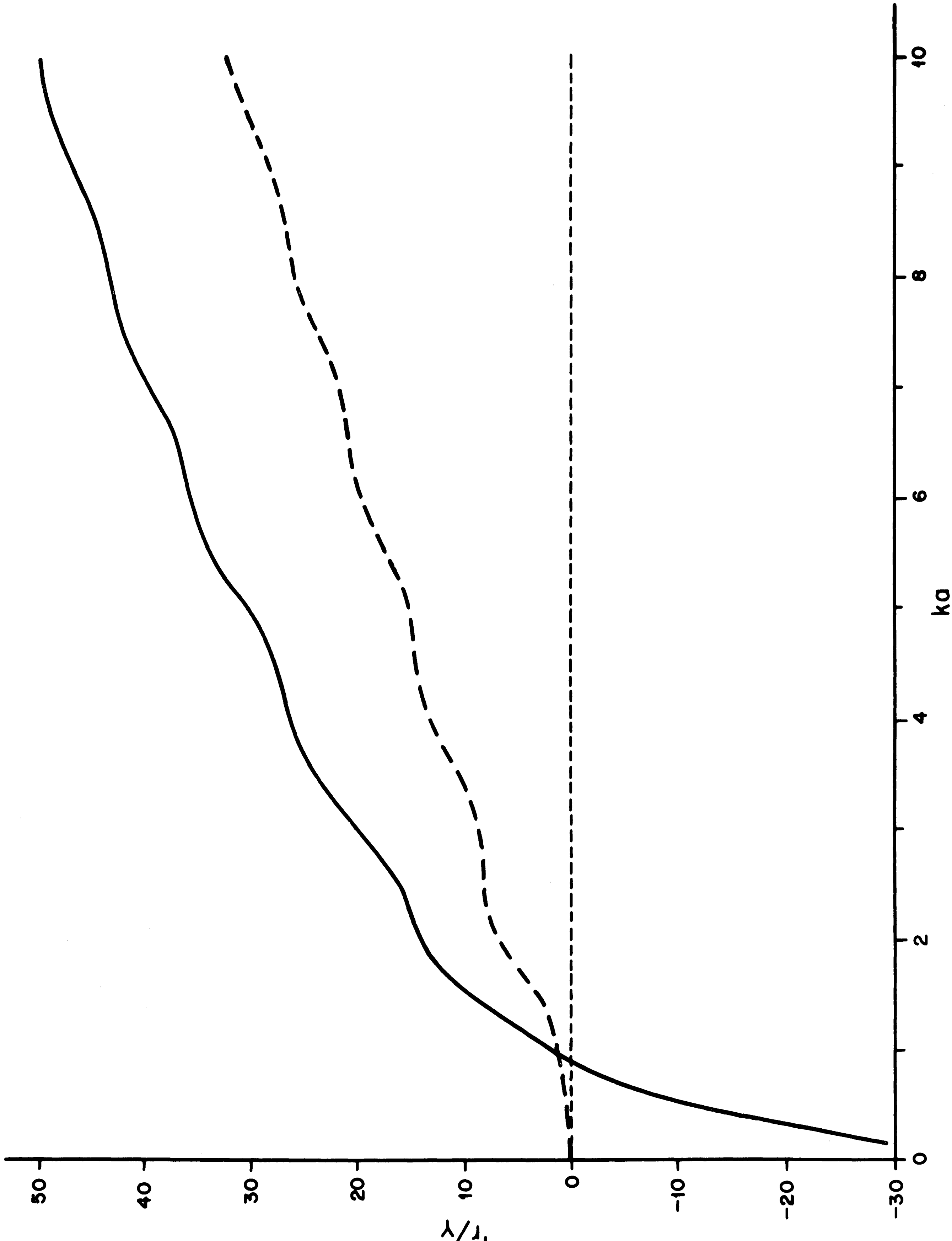

FIG. 6: REAL (---) AND IMAGINARY (—) PARTS OF NORMALIZED RADIATION ADMITTANCE FOR $\theta_o = 90^o$ AND $\delta = 0.0392$.

oscillation as ka increases. The imaginary parts, on the other hand, have a negative singularity for ka = 0, but as a consequence of the asymmetric excitation of the slot, their signs change from negative to positive at a value of ka near to unity. For larger ka, the curves for the imaginary parts lie almost parallel to and above those for the real parts.

The value of δ used in the above computations was determined by the equivalent slot width in the experimental model discussed in Section V, but to investigate the effect which a change of slot width has on the radiation admittance, Y_r/Y was computed for $\delta = 0.02(0.02)0.24$ with ka = 4.28 and $\theta_o = 90^o$. As can be seen from Figure 7, the real part is essentially constant for the full range of δ considered, but the imaginary part shows a significant variation. Because of the increasing local capacitance in the region of the gap as δ approaches zero, the imaginary part has a positive singularity at $\delta = 0$, and is monotonically decreasing as δ increases.

Having computed or available $S_1^s(0)$, $T_2(\theta_o)$ and Y_r/Y it is now possible to determine the loading admittance necessary for zero back scattering, and in Figures 8 through 10 the real and imaginary parts of Y_ℓ/Y based on equation (51) are plotted as functions of ka for $\theta_o = 60^o$, 90^o and 120^o respectively. Taking, for example, Figure 8, we observe that the curves for both the real and imaginary parts are quite irregular in structure and, as $ka \rightarrow 0$, Im. $Y_\ell/Y \rightarrow \infty$. Of the two curves, however, the one for the real part is the more interesting because of its greater practical significance. Bearing in mind that all non-negative values of Re. Y_ℓ correspond to passive loads, it is apparent that zero back scattering is achievable using only a passive load for all ka less than (about) 2.9. At this value of ka the curve for Re. Y_ℓ crosses the zero line and stays negative until ka reaches 6.6(approx.), at which time it becomes positive again. This oscillatory pattern continues out to the largest ka computed, and for every ka such that Re. $Y_\ell \geq 0$, passive loading is sufficient to annul the back scattered field. In view of the later experimental study, it is remarked that the loading is purely susceptive whenever Re. $Y_\ell = 0$.

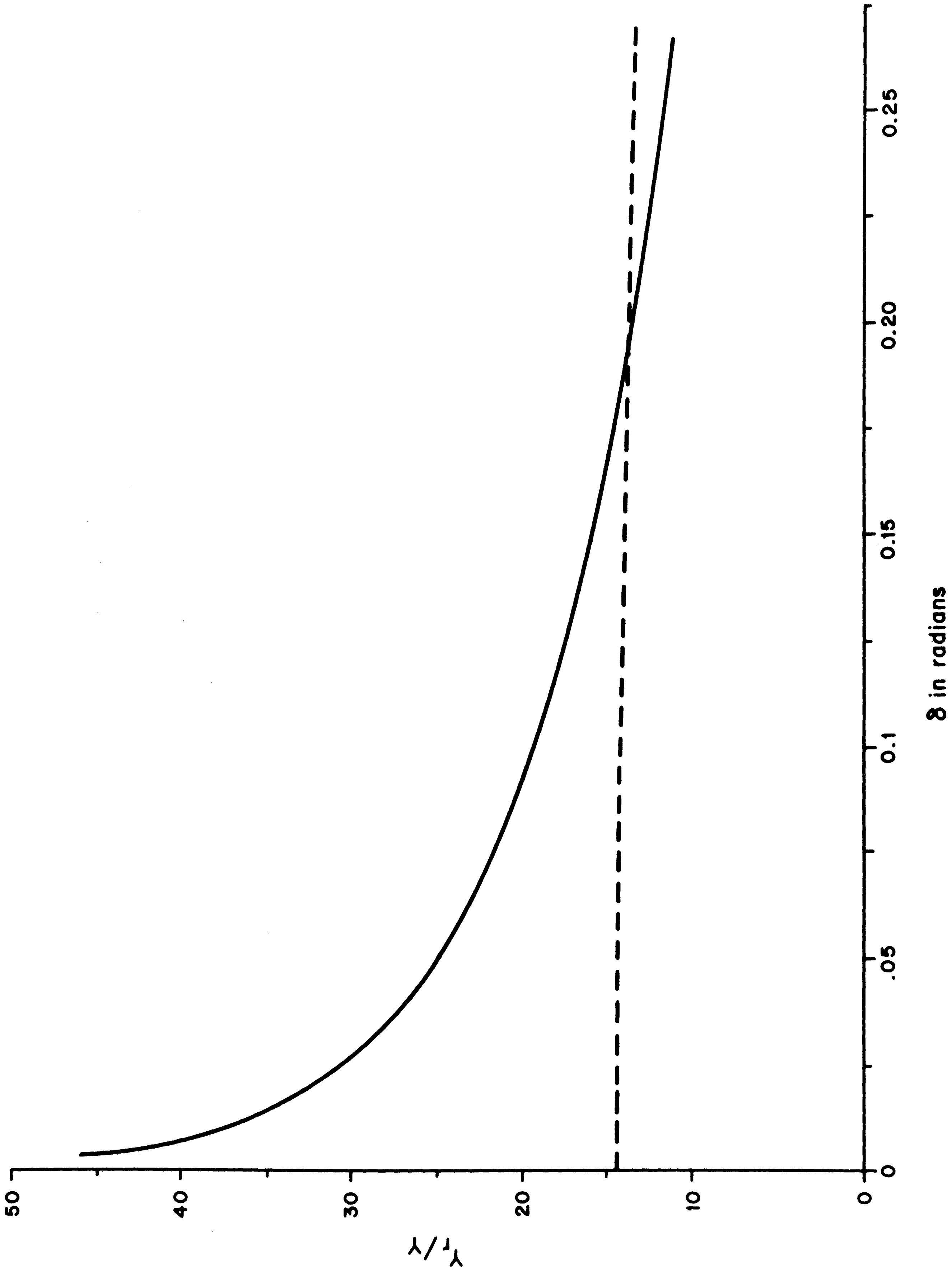

FIG. 7: REAL (---) AND IMAGINARY (—) PARTS OF NORMALIZED RADIATION ADMITTANCE FOR ka=4.28 AND $\theta_o = 90^o$.

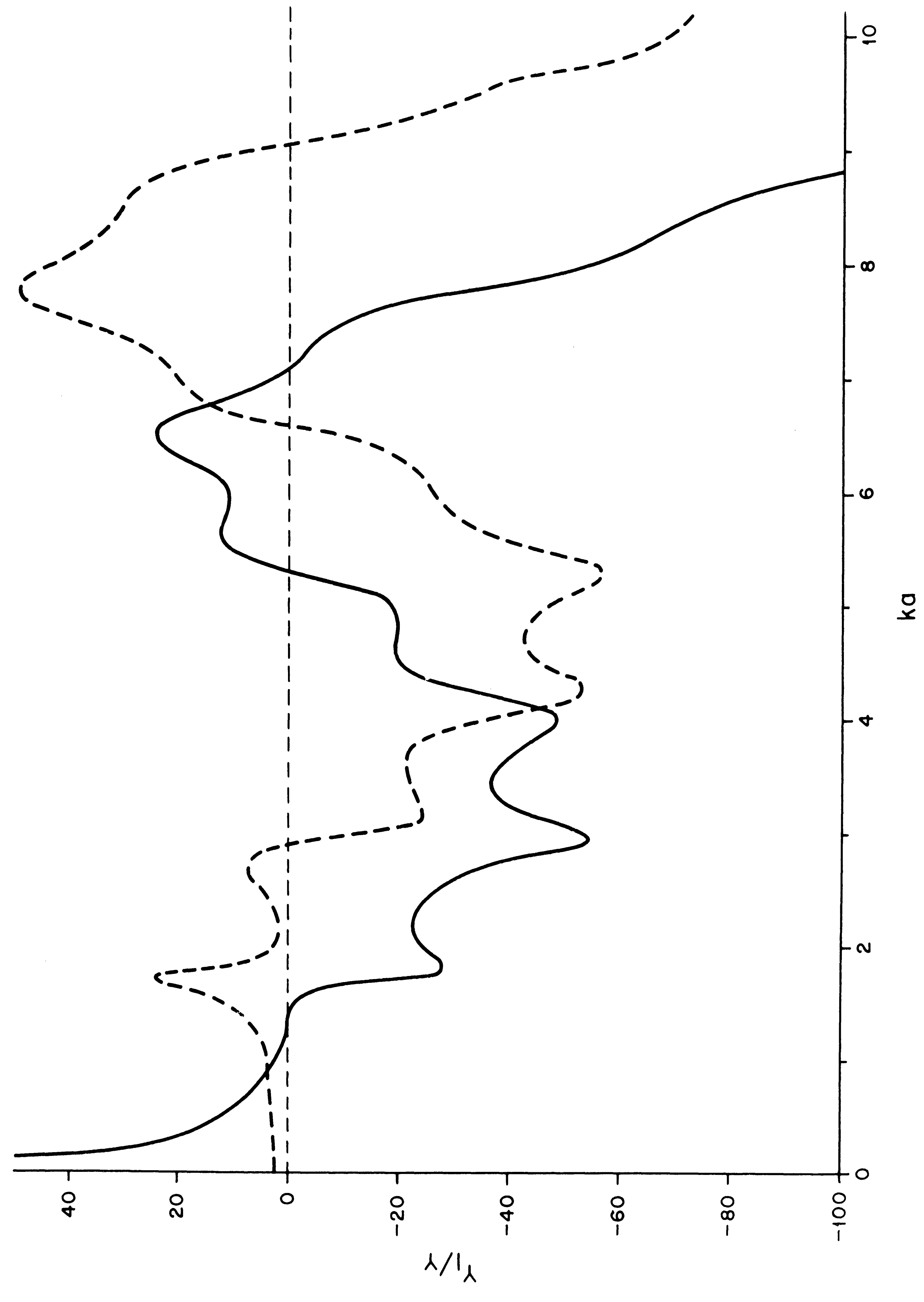

FIG. 8: REAL (---) AND IMAGINARY (—) PARTS OF NORMALIZED LOADING ADMITTANCE FOR ZERO BACK SCATTERING WITH $\theta_o = 60^o$.

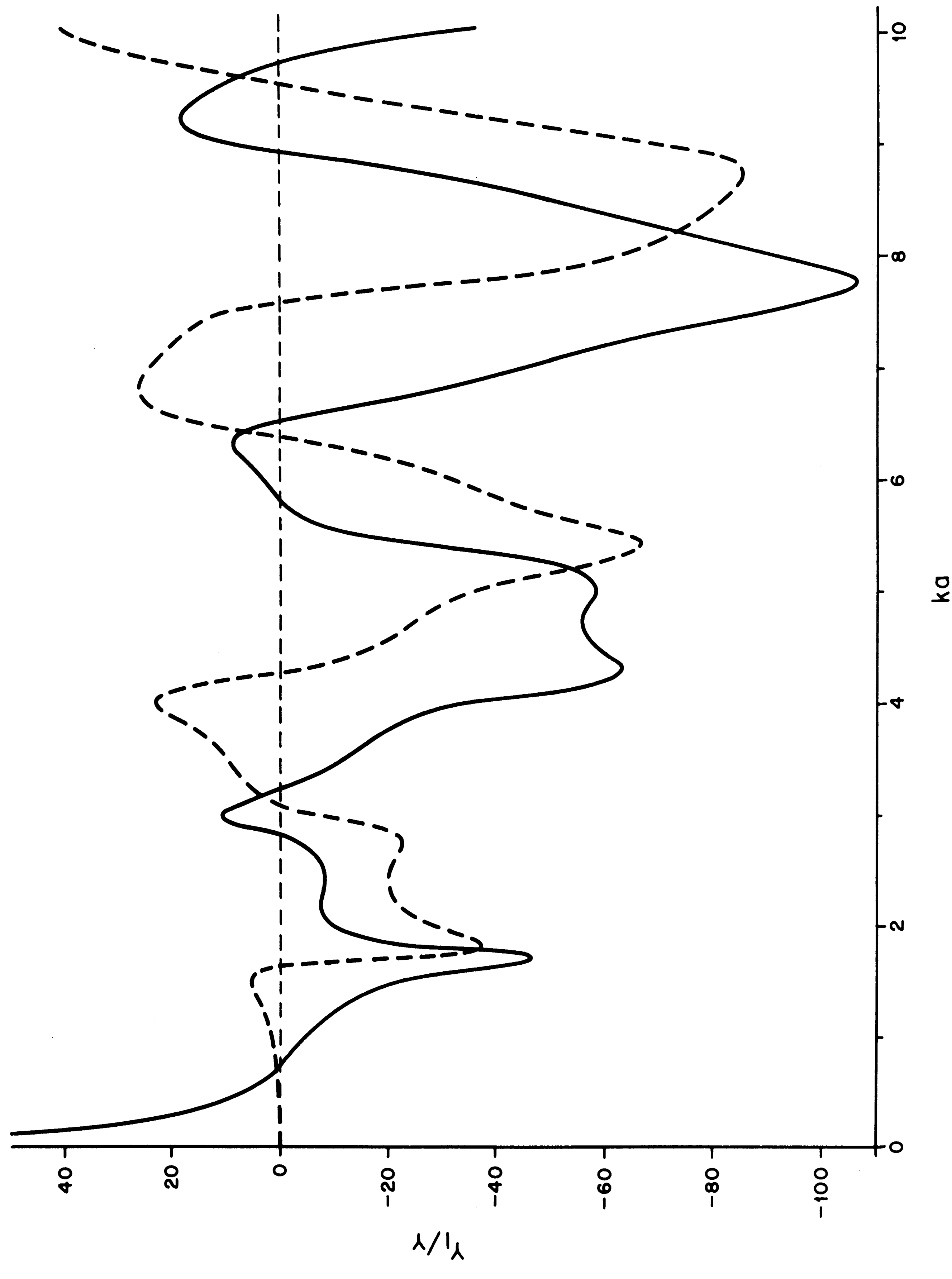

FIG. 9: REAL (---) AND IMAGINARY (——) PARTS OF NORMALIZED LOADING ADMITTANCE FOR ZERO BACK SCATTERING WITH $\theta_o = 90^o$.

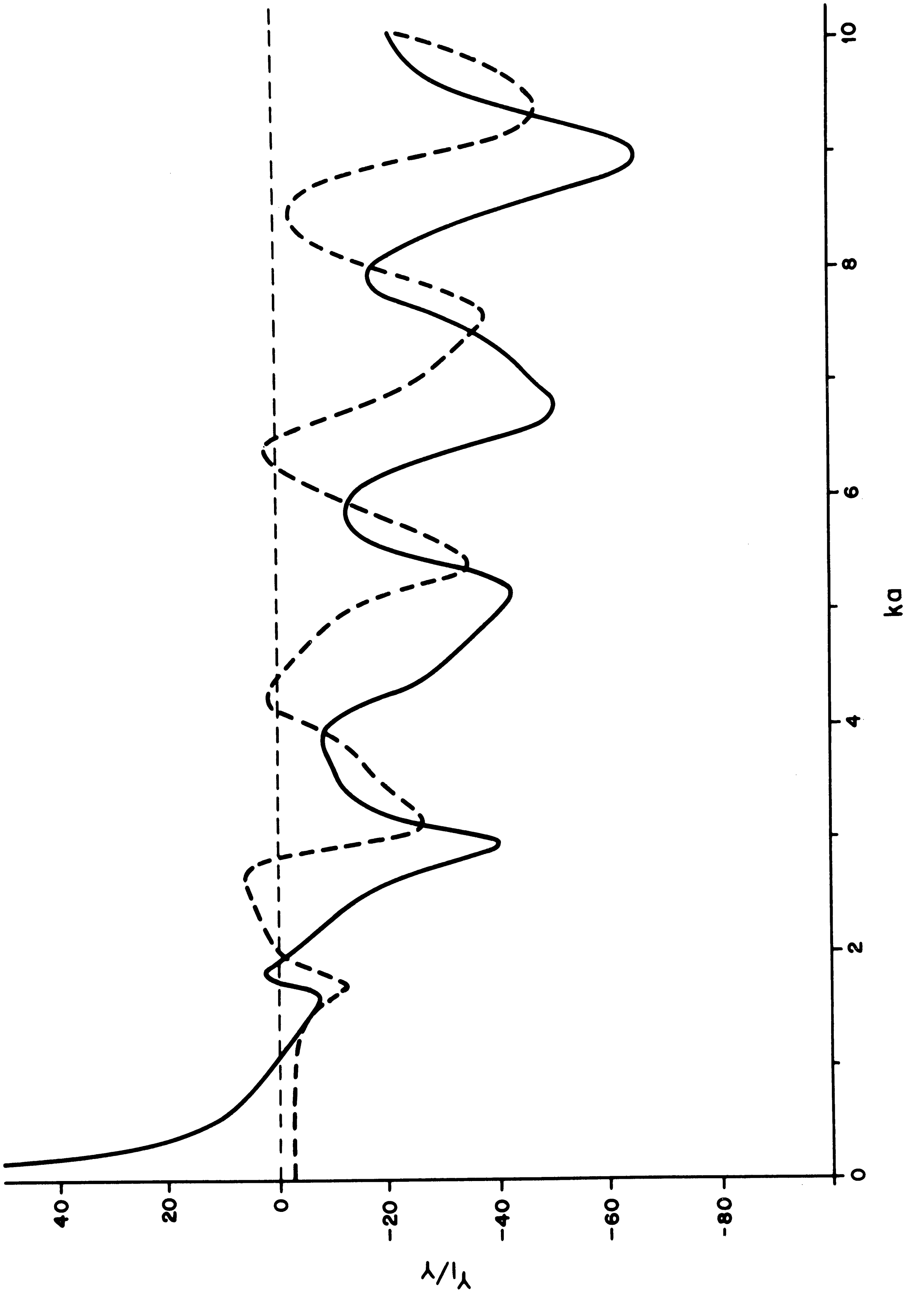

FIG. 10: REAL (---) AND IMAGINARY (—) PARTS OF NORMALIZED LOADING ADMITTANCE FOR ZERO BACK SCATTERING WITH $\theta_o = 120^o$.

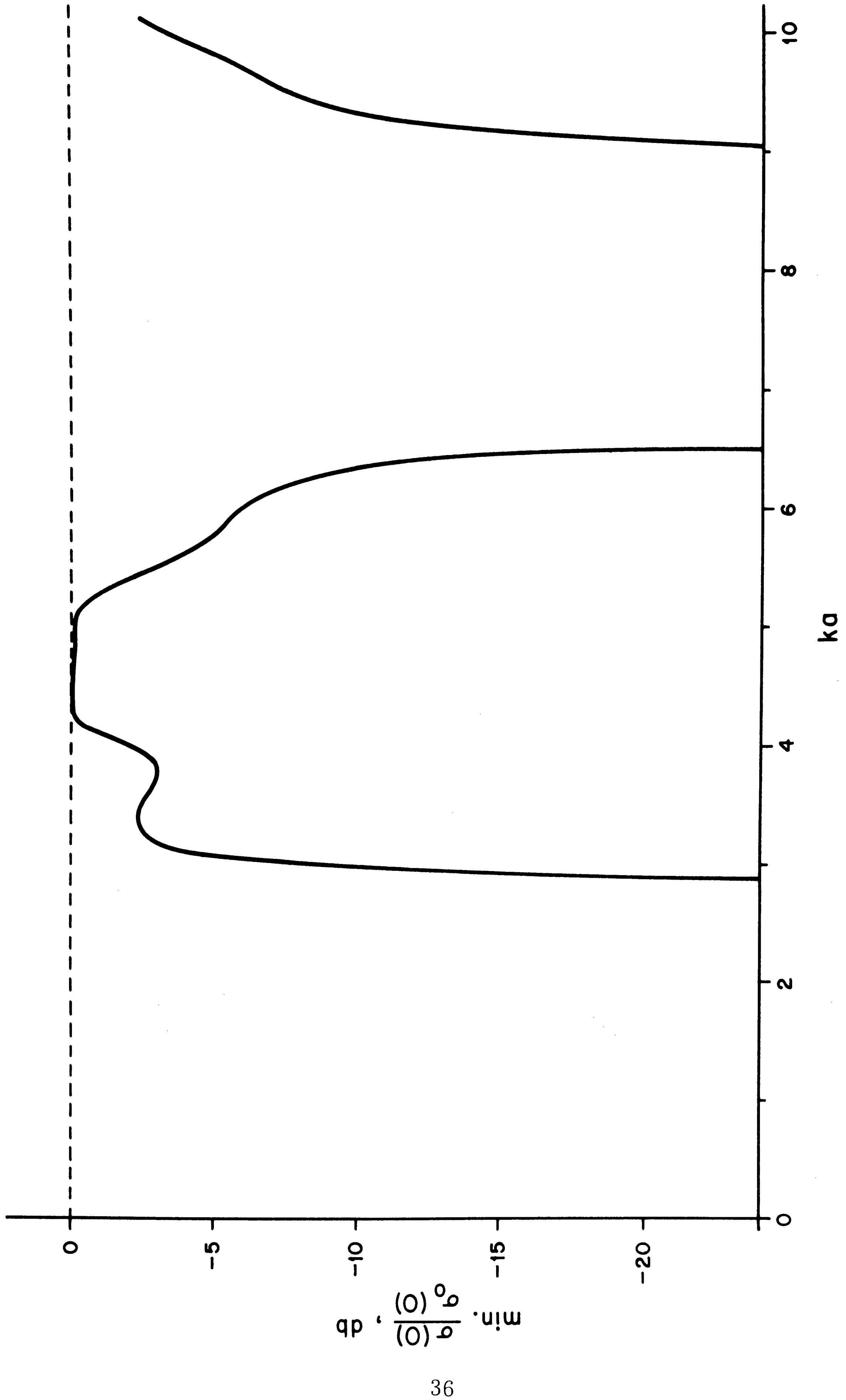

FIG. 11: MINIMUM RELATIVE BACK SCATTERING CROSS SECTION FOR PASSIVE LOADING AT $\theta_o = 60^o$.

Since passive loading is of most practical interest, let us consider the maximum and minimum back scattering cross sections that are obtainable in this manner. From equations (16), (46) and (50), the cross section $\sigma(0)$ of the loaded sphere, relative to the cross section $\sigma_o(0)$ of the unloaded body, can be written as

$$\frac{\sigma(0)}{\sigma_o(0)} = \left| 1 + \frac{\gamma_1 + i\gamma_2}{x_1 + i x_2} \right| , \tag{59}$$

where

$$\gamma_1 + i\gamma_2 = \frac{\pi\left\{ka \sin\theta_o T_2(\theta_o)\right\}^2}{2 S_1^s(0)} \tag{60}$$

and

$$x_1 + i x_2 = \frac{Y_\ell}{Y} + \frac{Y_r}{Y} , \tag{61}$$

with γ_1, γ_2, x_1 and x_2 real. The minimum and maximum values of the above cross section ratio for

$$x_1 = \text{Re.} \frac{Y_r}{Y} \equiv b > 0$$

are now given by the formulae in Appendix A, and with a passive slot at $\theta_o = 60^o$ the results are as shown in Figures 11 and 12. Taking first the minima, the return is zero for $ka \leq 2.9$; then, as Re. Y_ℓ in Figure 8 swings from positive to negative, the minimum return increases from zero and rises rapidly to a peak value only infinitesimally less than the return from the unloaded sphere, before falling back to zero again. The pattern is repeated, apparently without end. If, on the other hand, we aim for a maximum return (Figure 12), an arbitrarily large enhancement can be achieved by taking ka sufficiently small, but as this is a consequence of the higher order zero of the normalizing function $\sigma_o(0)$ at $ka = 0$ the result is somewhat misleading. For ka greater than (say) 0.5, however, the enhancement is genuine, and Figure 12 shows that an increase of as much as 19.4 db can be obtained for a particular value of ka, with an average enhancement of more than 10 db for the range $1.0 \leq ka \leq 10.0$.

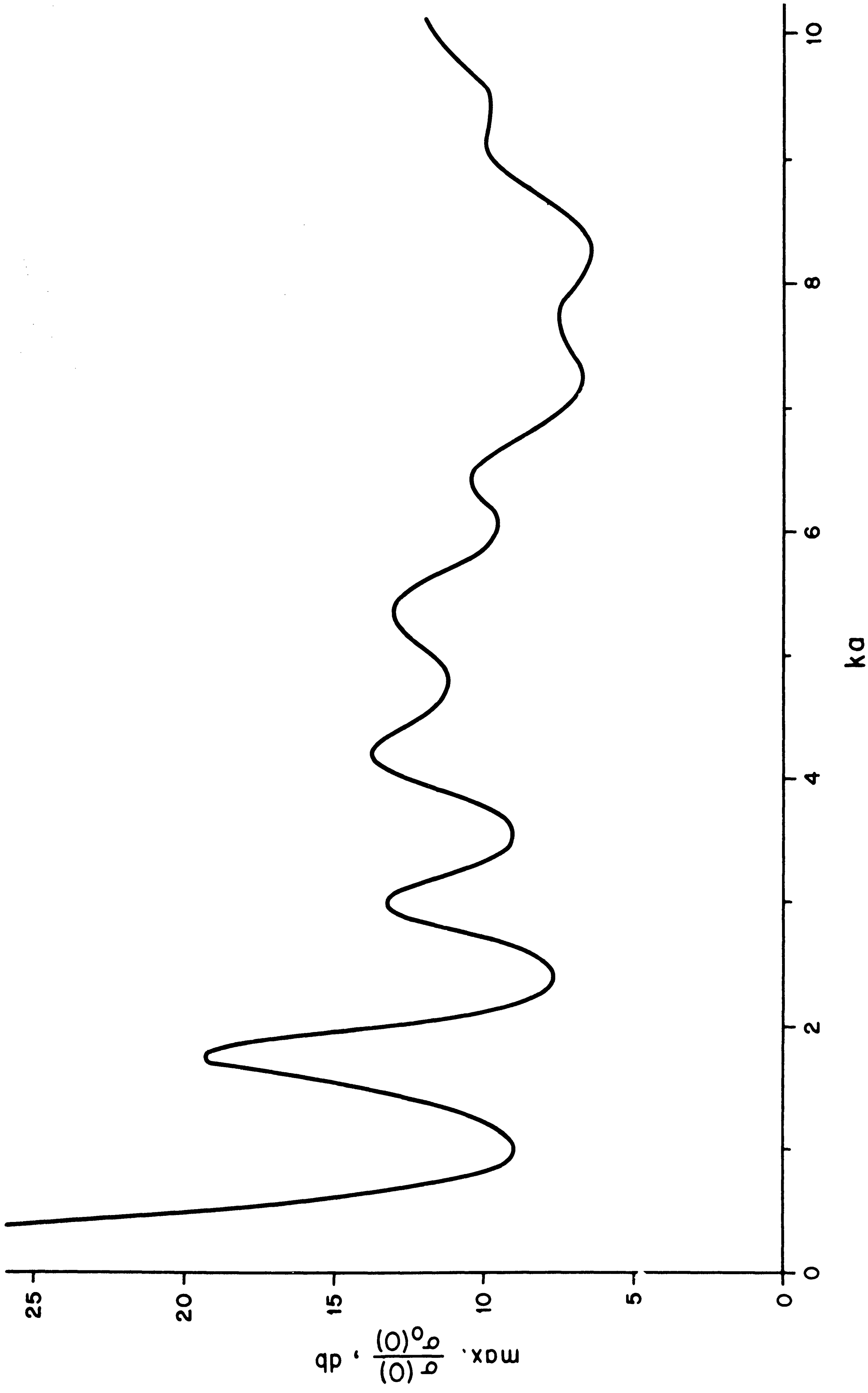

FIG. 12: MAXIMUM RELATIVE BACK SCATTERING CROSS SECTION FOR PASSIVE LOADING AT $\theta_o = 60^o$.

The analogous data for slots at 90° and 120° is presented in Figures 13 through 16, and though the qualitative behavior is similar to that described above, the displacement of the slot towards and into the shadow region decreases markedly the control that can be had with passive loading. Thus, for example, with the slot at 120° a zero cross section is possible only for very limited ranges of ka, with the first range not commencing until ka = 1.99. The maximum enhancement is also decreased, and averages a mere 4.7 db for $1.0 \leq ka \leq 10.0$.

To illustrate the bistatic performance of a loaded sphere, the case ka = 4.28 and $\theta_0 = 90^\circ$ has been investigated, with a loading $Y_\ell / Y = -i\,63.45$ (purely susceptive) necessary to give zero back scattering. The radiated far field amplitudes $S_1^r(\theta)$ and $S_2^r(\theta)$ were evaluated at 5° intervals from $\theta = 0^\circ$ to 180°, and the total scattering amplitudes obtained from equations (46) and (47). To simplify the computations, the bistatic cross sections were normalized relative to the back scattering cross section $\sigma_0(0)$ of the unloaded sphere, and for ease of presentation, attention will be confined to E-plane (ϕ=0) and H-plane ($\phi = \pi/2$) scattering. The results are given in Figures 17 and 18 respectively.

Because of the choice of loading there is complete cancellation of the return for $\theta = 0$, and the null widths (between 3 db points) in the E- and H-planes are 36° and 60° respectively. Beyond the nulls there is, on average, a slight enhancement of order 1 db in the scattered field, and it is tempting to conclude from this that any power removed from directions near $\theta = 0$ must be redistributed amongst the other angles. Such a redistribution, however, is by no means essential. For different values of ka and θ_0 it is possible that the loading for zero back scattering would also produce a reduction in most other directions as well, but if the real aim is to decrease the overall pattern, the choice of loading should be based on a criterion specifically developed for the reduction of the total (i.e. integrated) scattering cross section. To judge from the results found for a thin cylinder (Chen and Liepa, 1964), it is possible that some decrease in the total scattering could be achieved with passive loading at least for the smaller values of ka.

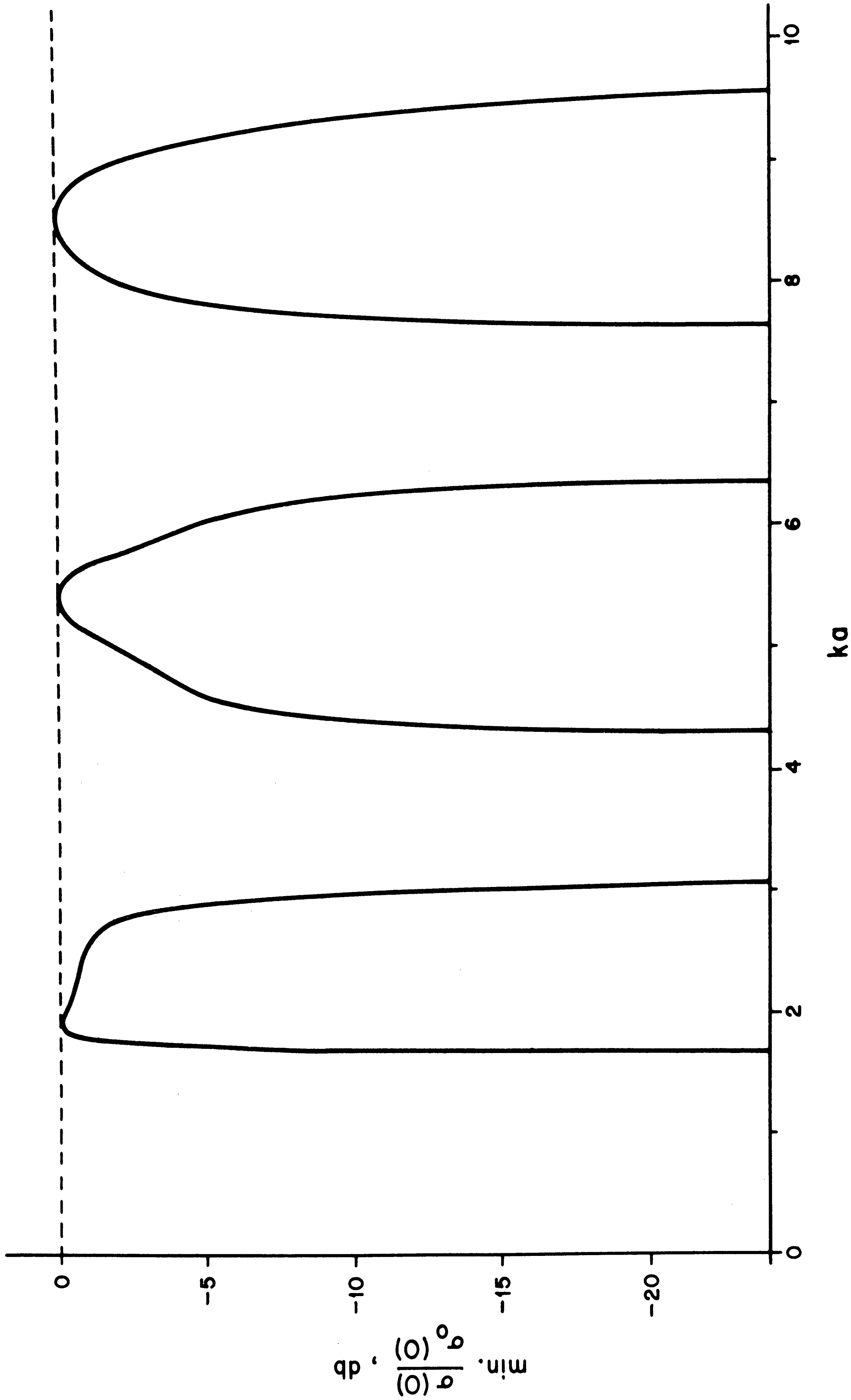

FIG. 13: MINIMUM RELATIVE BACK SCATTERING CROSS SECTION FOR PASSIVE LOADING AT $\theta_o = 90^{\circ}$.

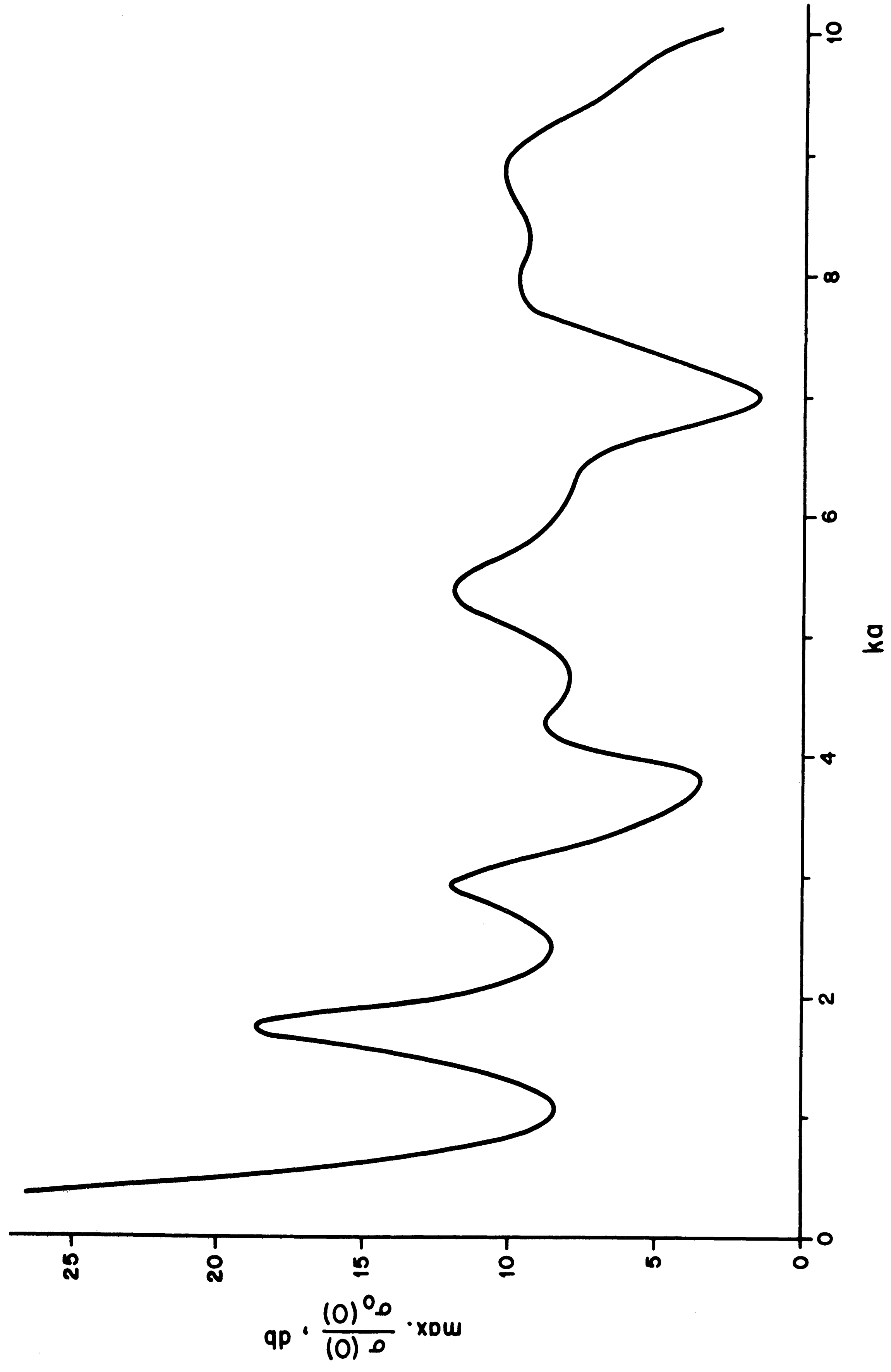

FIG. 14: MAXIMUM RELATIVE BACK SCATTERING CROSS SECTION FOR PASSIVE LOADING AT $\theta_o = 90^o$.

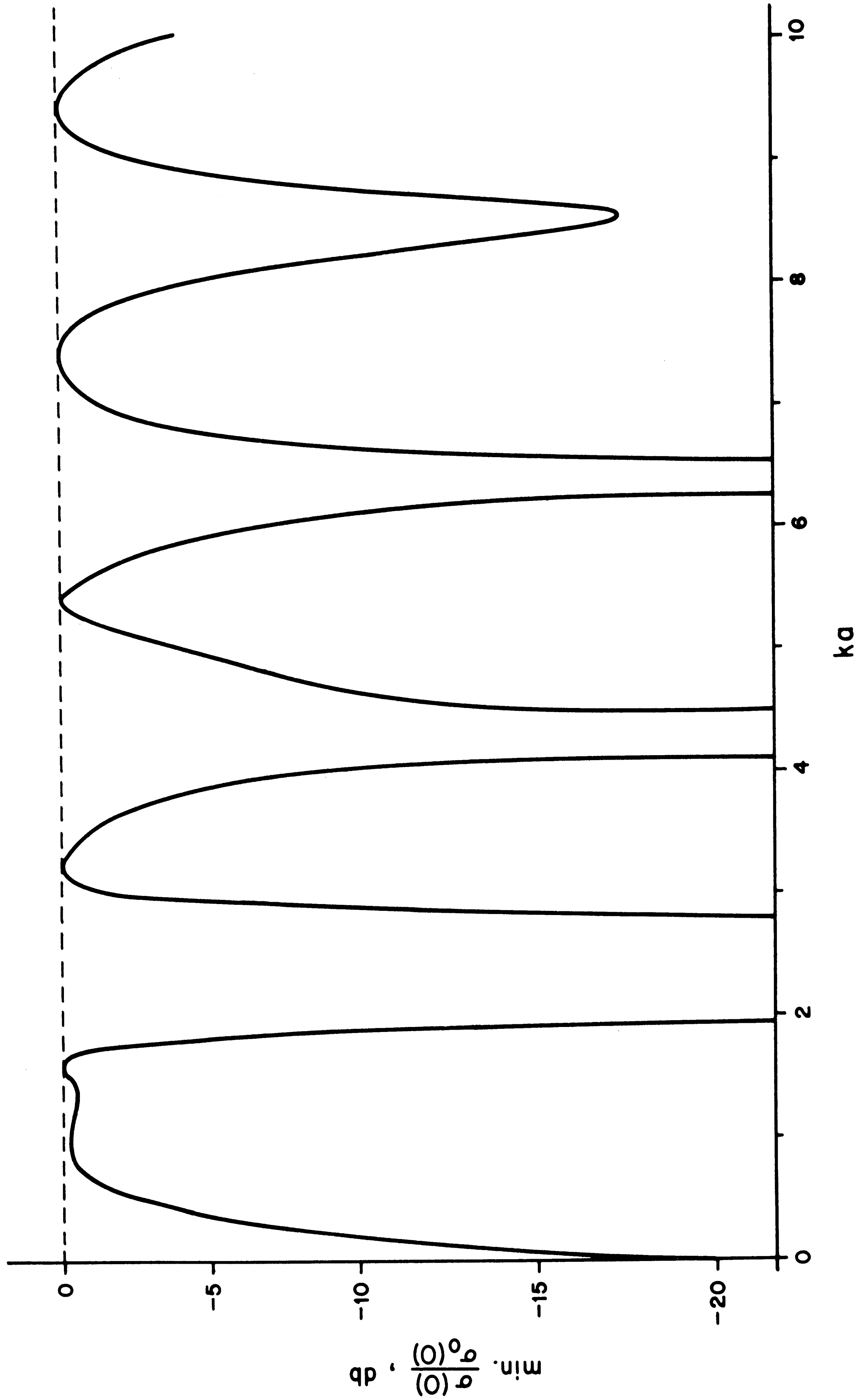

FIG. 15: MINIMUM RELATIVE BACK SCATTERING CROSS SECTION FOR PASSIVE LOADING AT $\theta_o = 120^o$.

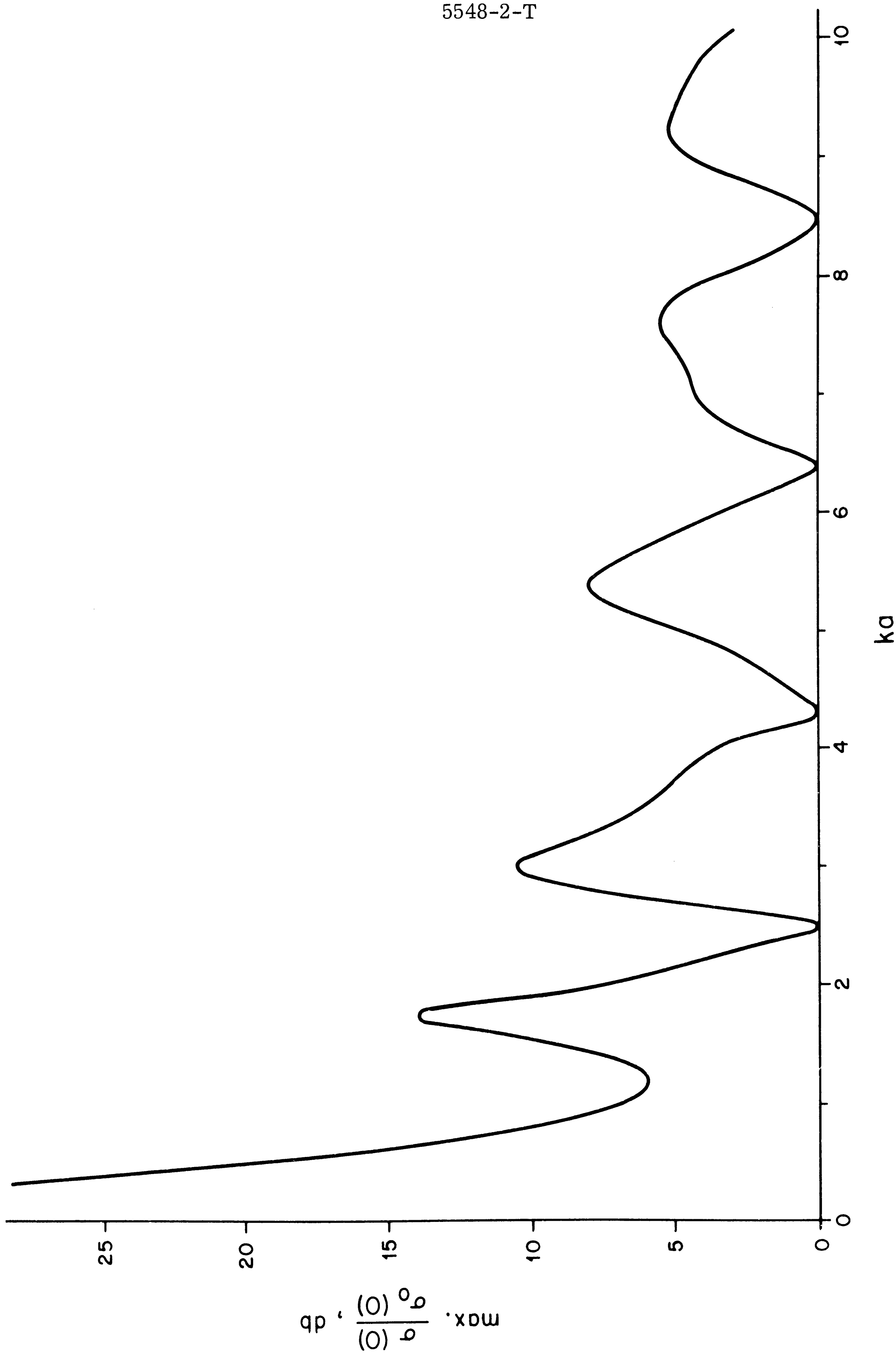

FIG. 16: MAXIMUM RELATIVE BACK SCATTERING CROSS SECTION FOR PASSIVE LOADING AT $\theta_o = 120^o$.

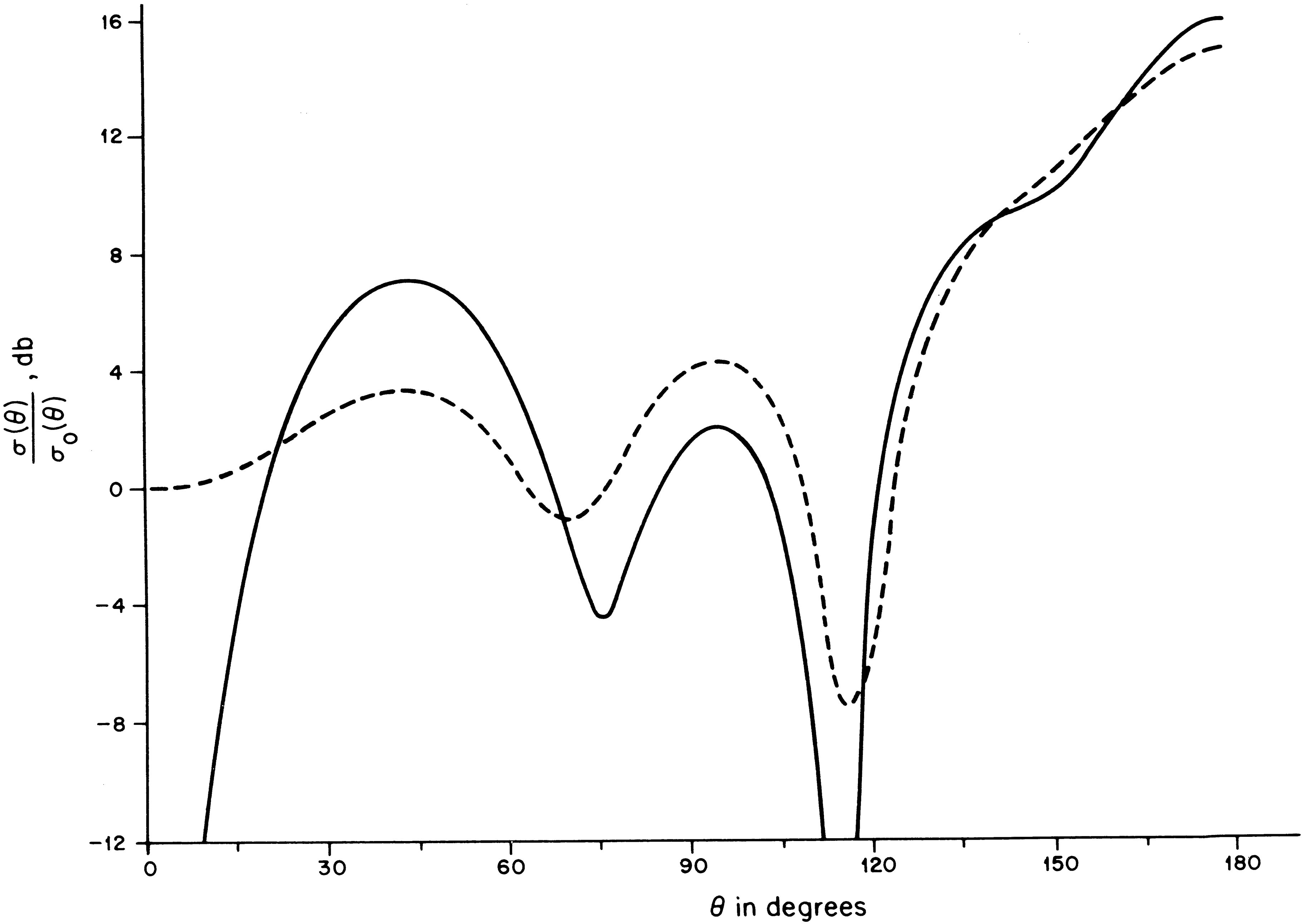

FIG. 17: RELATIVE BISTATIC SCATTERING CROSS SECTIONS IN E-PLANE ($\emptyset$=0) FOR LOADED (—) AND UNLOADED (---) SPHERE: ka=4.28, $\theta_o = 90^o$ AND $Y_\ell = -i63.45\, \bar{Y}$.

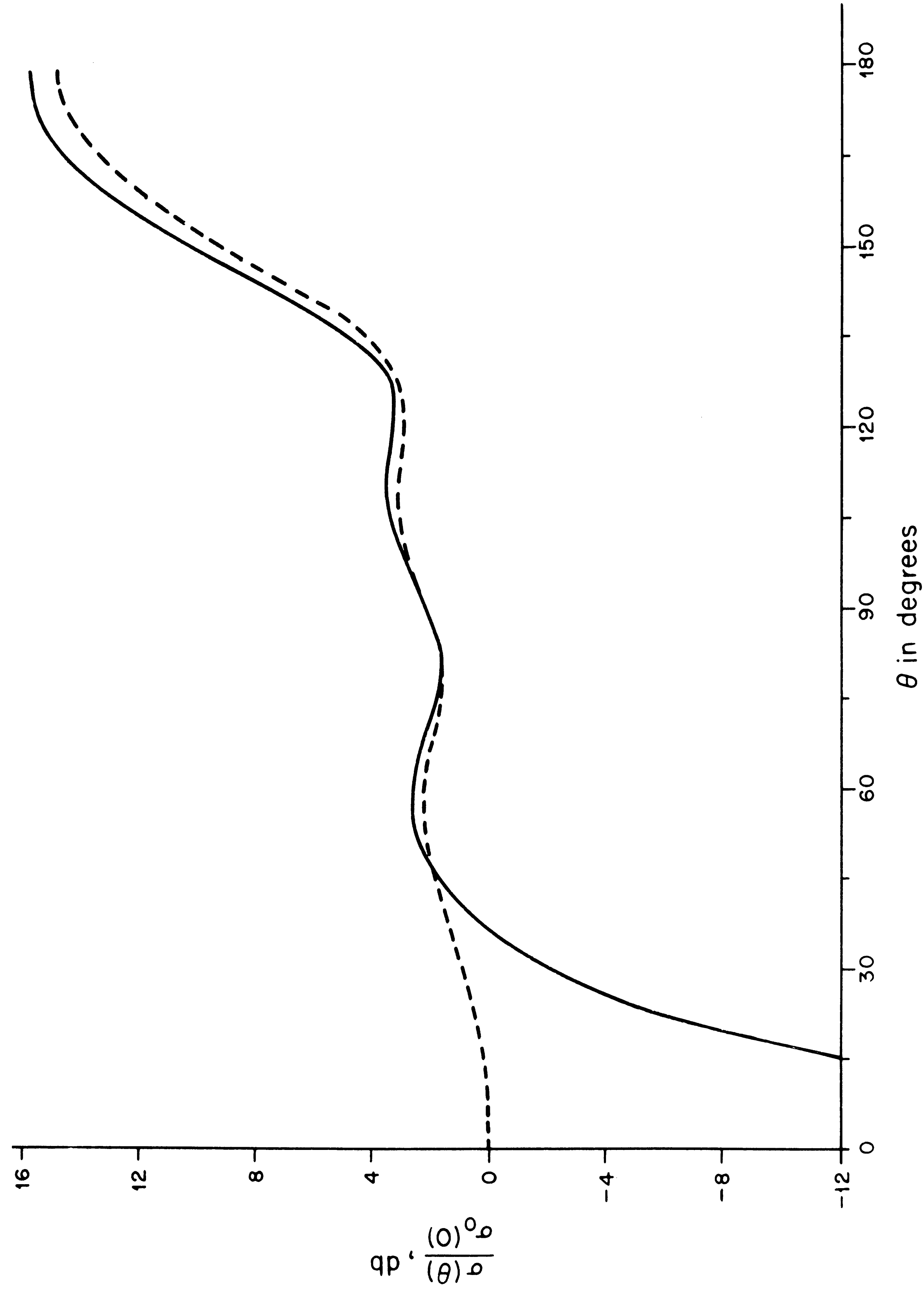

FIG. 18: RELATIVE BISTATIC SCATTERING CROSS SECTIONS IN H-PLANE ($\phi = 90^o$) FOR LOADED (—) AND UNLOADED (– –) SPHERE: ka=4.28, $\theta_o = 90^o$ AND $Y_{\ell} = -i63.45\ Y$.

V
EXPERIMENT

To confirm the above predictions of the back scattering behavior, a series of measurements were performed using a sphere with a circumferential cavity-backed slot. A photograph and sketch of the model are given in Figures 19 and 20 respectively. The model consisted of two identical solid aluminum caps joined together by means of a partially-threaded shaft at the center. The spacing or gap between the caps formed a radial cavity with input at the outer (sphere) radius and a short at the inner radius. Whereas the outer radius of the cavity was identical to that of the sphere itself, the inner radius was determined by the size of the shorting disc used. In all, a total of 21 discs were available, and with these the inner diameters could be varied from 0.3125 (the diameter of the shaft joining the caps) to 3.133 inches. The discs were made from 1/16 inch sheet aluminum. With the exception of an outer rim, each had a slight undercut in thickness to give better electrical contact, and when in place the two caps conformed to a spherical surface of diameter 3.133 inches everywhere except for the equatorial slot. The surface width of the slot subtended an angle of approximately 2.25^{o} at the center of the sphere.

The back scattering measurements were made at frequencies 2.808, 3.605, 3.709, 3.838 and 5.136 Gc, corresponding to which ka = 2.340, 3.004, 3.090, 3.198 and 4.280 respectively. The equipment was that generally used in cw scattering experiments except that the conventional azimuth-amplitude recorder was replaced by a HP 415 B meter for greater accuracy of reading. A block diagram of the equipment is given in Figure 21. The distance from the antenna to the pedestal was approximately 25 feet, and the sphere was placed on the pedestal with the plane of the slot perpendicular to the direction of the incident, horizontally polarized, wave.

At each frequency the back scattering cross section was measured for a series of shorting discs, with calibration relative to the return from the unloaded sphere. The resulting normalized cross sections are listed in Table 1, and in Figures 22 through 26 the data is plotted as functions of the imaginary part of Y_{ℓ}/Y.

FIG. 19: EXPERIMENTAL MODEL

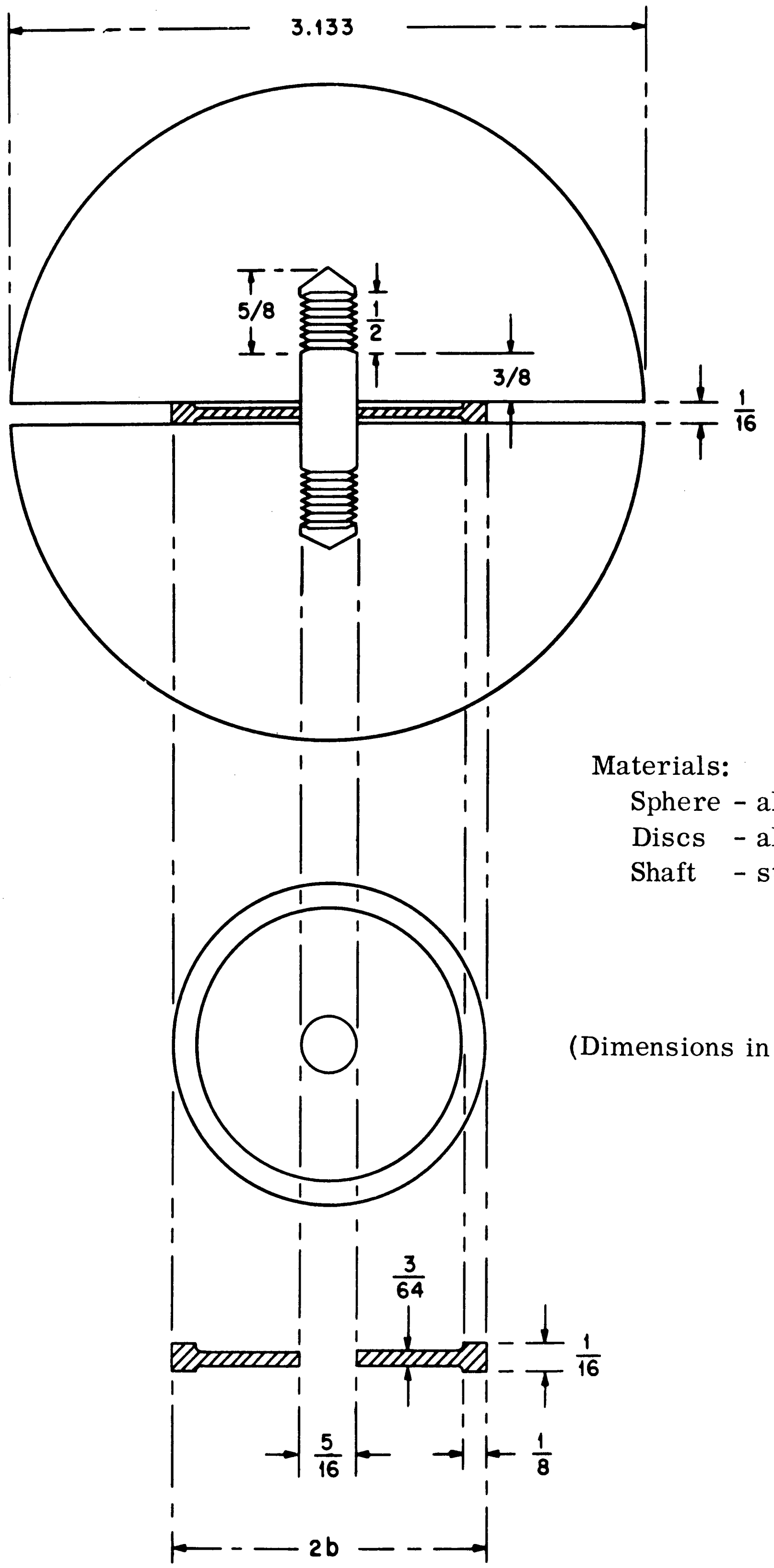

2b
0.500
0.625
0.750
0.875
1.000
1.125
1.250
1.375
1.500
1.625
1.750
1.875
2.000
2.125
2.250
2.375
2.500
2.625
2.750
2.875
3.133

Materials:
- Sphere - aluminum
- Discs - aluminum
- Shaft - steel

(Dimensions in inches)

FIG. 20: SECTORIAL VIEW OF MODEL

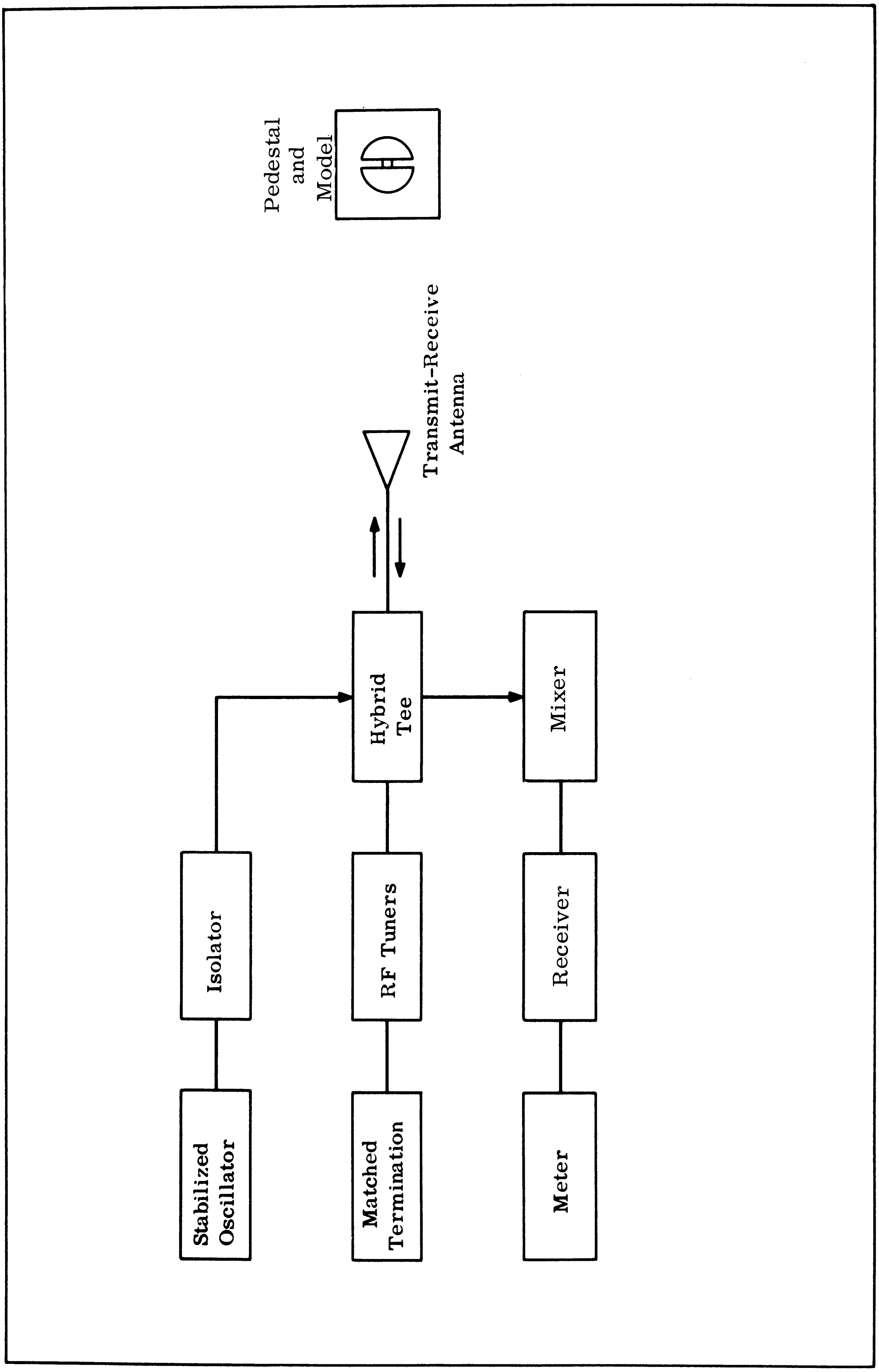

FIG. 21: BLOCK DIAGRAM OF EQUIPMENT

TABLE 1: EXPERIMENTAL DATA

Shorting disc diameter 2b, inches	Relative Return,* db				
	2.808 Gc	3.605 Gc	3.709 Gc	3.838 Gc	5.136 Gc
.3125	-0.7	-1.5	-0.7	-0.8	
.500	-0.8	-1.7	-1.7	-1.1	
.625	-0.7	-1.9	-1.8		
.750	-0.7	-2.3		-1.3	
.875	-0.6	-2.5	-2.5	-1.6	
1.000	0.0	-3.3	-2.5		
1.125	2.3	-3.8	-3.0	-2.0	
1.250	7.5	-5.6	-3.5	-2.4	1.3
1.375	6.1	-8.0	-5.6	-3.4	
1.500	3.2	-13.4	-9.4	-4.6	1.9
1.625	2.2	-0.8	-14.7	-9.6	2.3
1.750	1.6	10.4	6.4	-5.4	2.8
1.875	1.3	7.0	7.0	7.0	3.7
2.000	1.0	4.5	4.4	4.3	5.3
2.125					8.2
2.250					-2.5
2.375					-11.7
2.500	0.5	1.4	1.0	1.1	-4.8
2.625					-2.8
2.750					-1.8
2.875					-1.0
3.133	0.0	0.0	0.0	0.0	0.0

*relative to the unslotted sphere

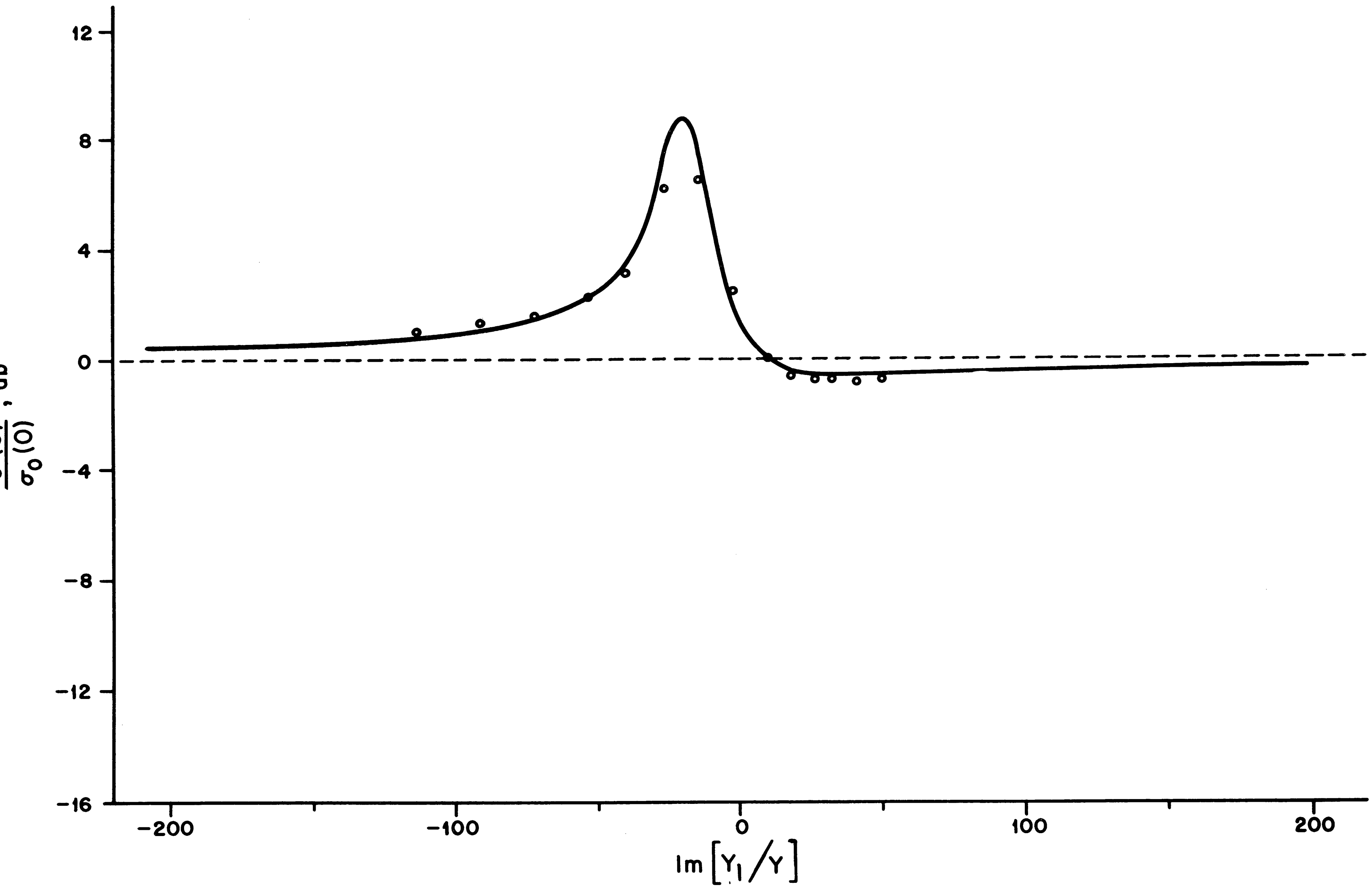

FIG. 22: THEORETICAL (—) AND EXPERIMENTAL (ooo) RELATIVE BACK SCATTERING CROSS SECTIONS WITH SUSCEPTIVE LOADING: ka=2.340 AND $\theta_o = 90^o$.

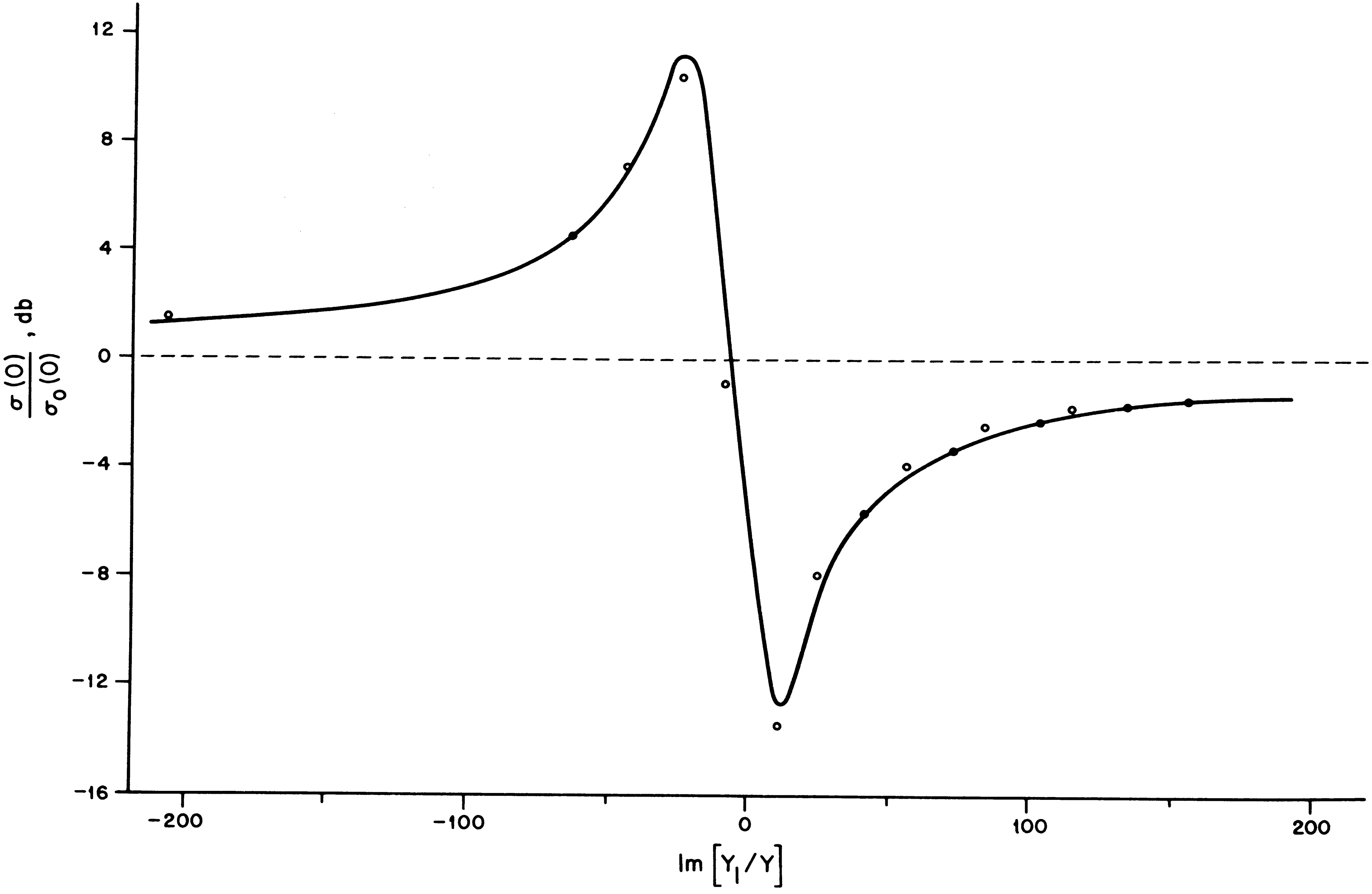

FIG. 23: THEORETICAL (—) AND EXPERIMENTAL (ooo) RELATIVE BACK SCATTERING CROSS SECTIONS WITH SUSCEPTIVE LOADING: ka=3.004 AND θ_o=90°.

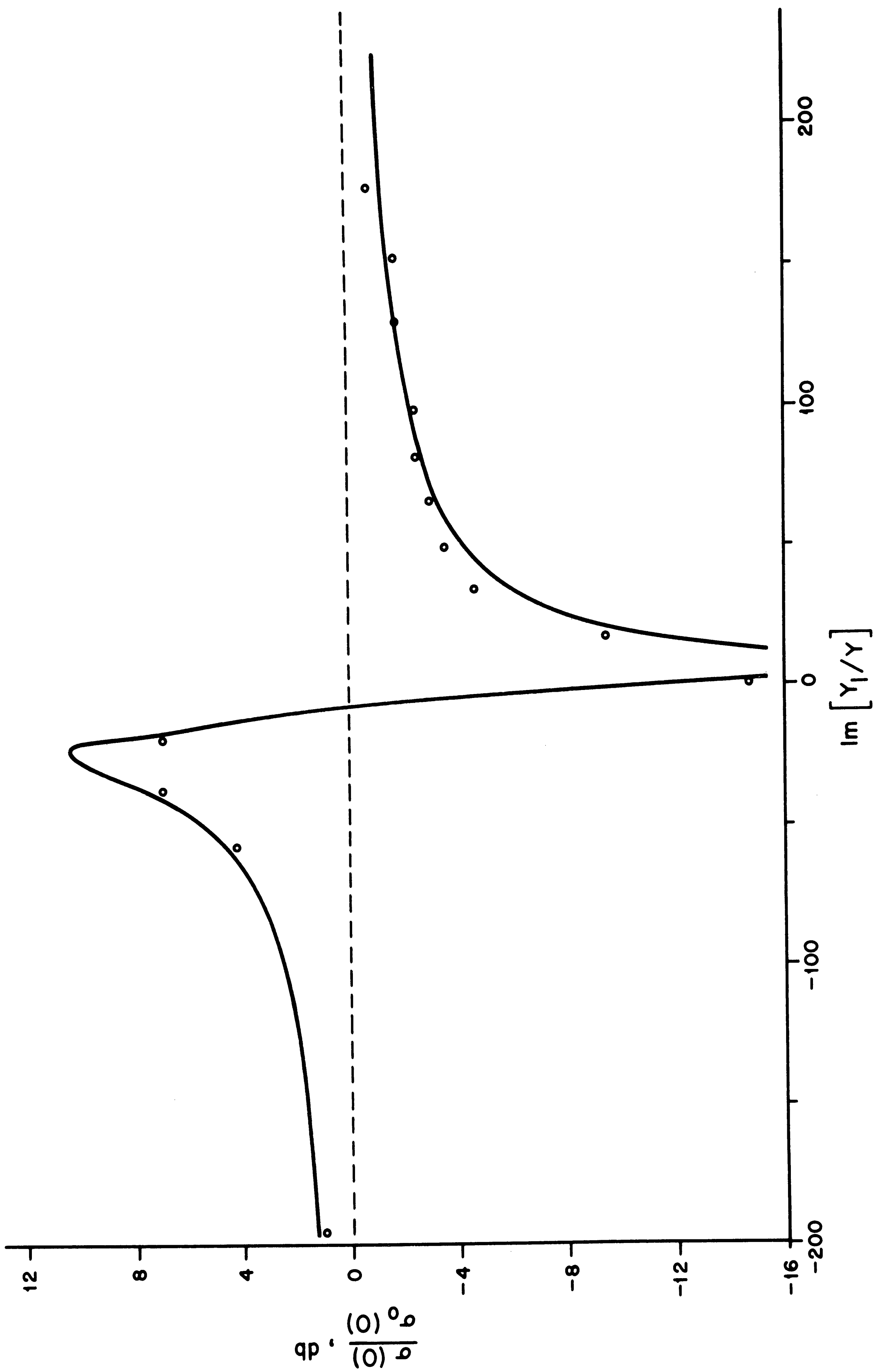

FIG. 24: THEORETICAL (—) AND EXPERIMENTAL (ooo) RELATIVE BACK SCATTERING CROSS SECTION WITH SUSCEPTIVE LOADING: ka=3.090 AND $\theta_o = 90^o$.

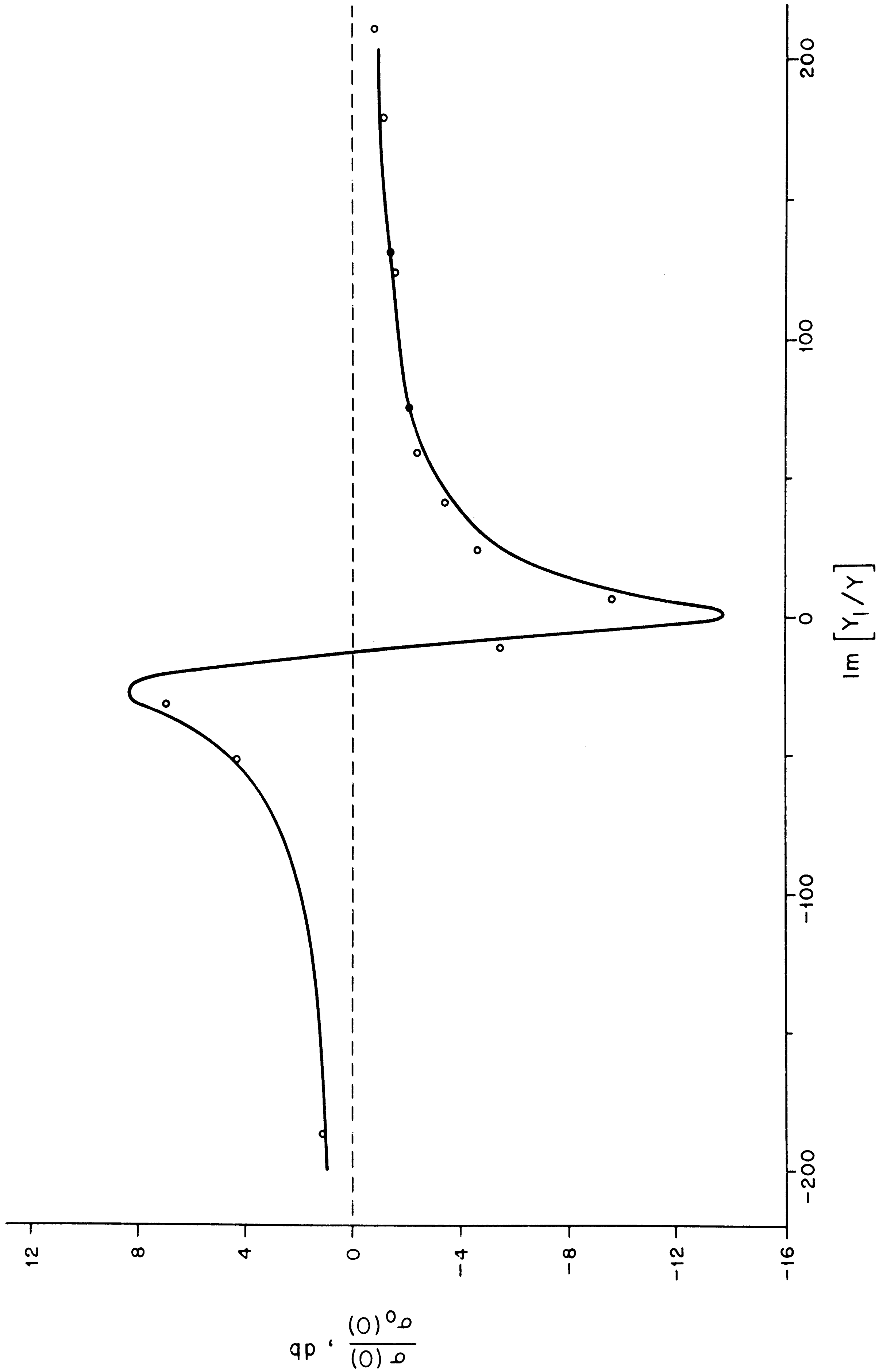

FIG. 25: THEORETICAL (—) AND EXPERIMENTAL (ooo) RELATIVE BACK SCATTERING CROSS SECTIONS WITH SUSCEPTIVE LOADING: ka=3.198 AND $\theta_o = 90^o$.

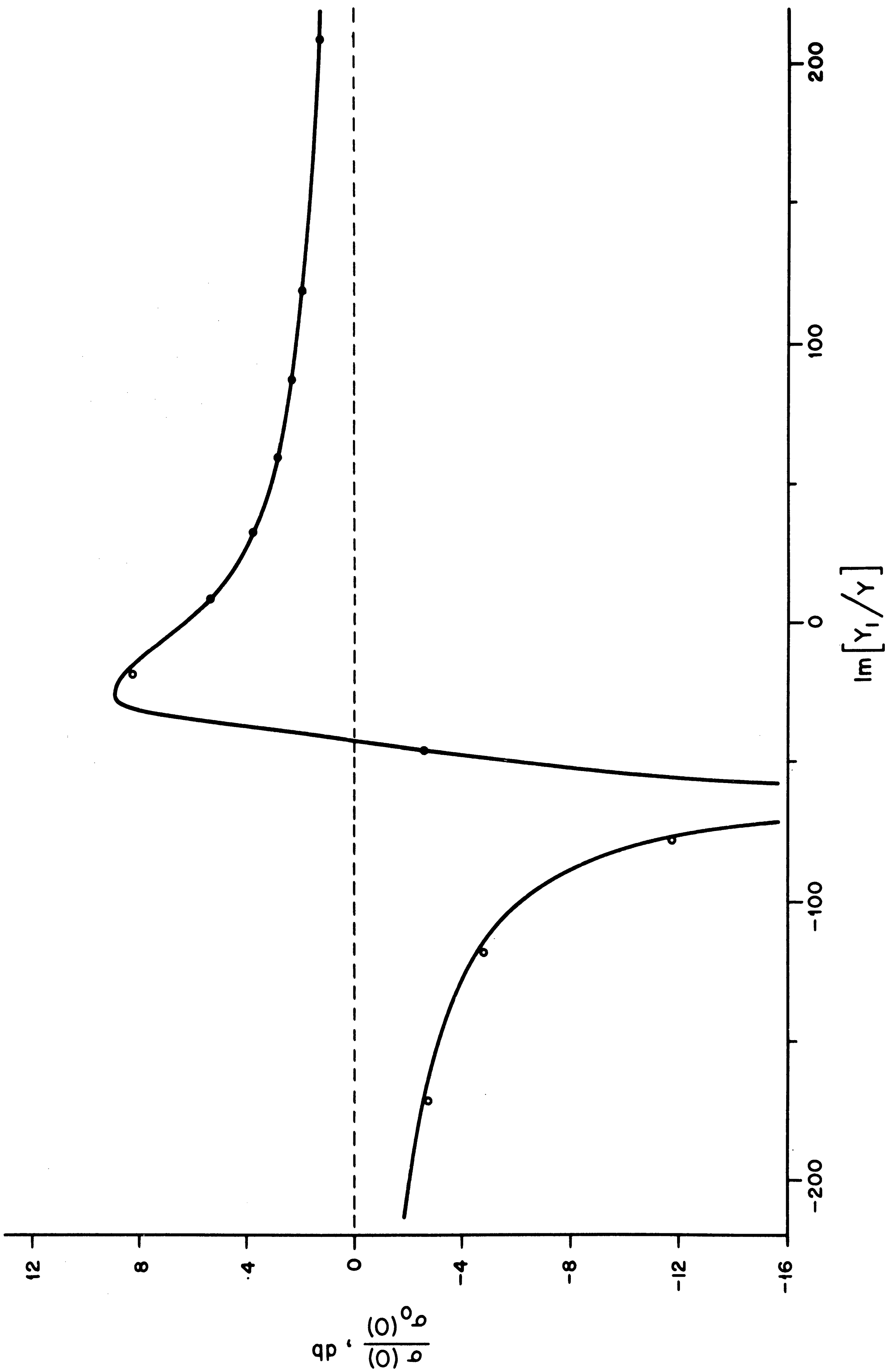

FIG. 26: THEORETICAL (—) AND EXPERIMENTAL (ooo) RELATIVE BACK SCATTERING SECTIONS WITH SUSCEPTIVE LOADING: ka=4.280 AND $\theta_o = 90^o$.

For this purpose, the disc diameters were converted to equivalent susceptive loadings using the formula in Appendix B. Also shown for comparison in Figures 22 through 26 are the theoretical curves computed from equation (46) with $\theta = 0$ and $\theta_o = 90^o$, and the agreement between theory and experiment is extremely gratifying.

The frequencies used in the above study were chosen to provide a reasonable sampling of the effects obtainable with susceptive loading only. Thus, for example, when ka = 2.340 zero back scattering would require a loading with large negative real part (see Figure 9) and this is, of course, unrealizable with a passive slot. In consequence, Figure 22 indicates no substantial cross section reduction (0.6 db at most), but an increase of 8.7 db is achieved for a particular Im. Y_ℓ, and since the maximum possible enhancement for this ka demands a susceptive loading, the peak level in Figure 22 is in agreement with Figure 14. Figures 23 through 25 show the results of 3 per cent changes in ka and span a range of ka within which a complete suppression of the back scattered field with susceptive loading occurs. In Figure 24 (ka = 3.090, corresponding to the second crossing of the zero line in Figure 9) the theoretical cross section for some small positive Im. Y_ℓ goes to zero. Experimentally, this particular loading was not obtainable with the available shorting discs, but for the disc which was nearest to this, the observed reduction in cross section was 14.7db. With a loading slightly less than this, the normalized cross section rose to a peak value of 10.3 db, and a similar peaking before the minimum is also apparent in Figure 23. On the other hand, at a frequency just greater than that for which a zero cross section can be obtained, the peak return occurs for a loading larger than that appropriate to the minimum (see Figure 25).

The final set of data in this group is presented in Figure 26 and is for ka = 4.280. This is yet another value for which susceptive loading gives complete cancellation, and the results are similar to those shown in Figure 24 except for the presence of the peak on the opposite side of the null. The changeover is attributable to the fact that the corresponding zero crossing in Figure 9 is now negative to positive as ka increases.

Although the analysis in Sections II and III was limited to the case of a field incident in a direction perpendicular to the plane of the slot, no such constraint existed in the experimental study, and it therefore seemed worthwhile to carry out a sample measurement of the back scattering cross section as a function of the rotation of the slotted sphere. The frequency selected was 5.136 Gc, corresponding to $ka = 4.280$, and to obtain the loading appropriate to the null in Figure 26 a new shorting disc of the requisite diameter was cut. The sphere was again mounted on the pedestal with the slot in a vertical plane, and measurements were made for both horizontal and vertical polarizations. The results are presented in Figures 27 and 28 along with the curves for the unloaded sphere. The large cross section reduction for incidence in the direction normal to the slot is clearly evident. For both polarizations the reduction is of order 20 db and though theoretically it should be infinite, the minor peaking at the center of each minimum could be due to the shorting disc being fractionally smaller than required. However, in view of the slightly differing magnitudes of the cross sections for zero rotation, a more likely source of the residual contribution is a sphere-pedestal interaction or a room effect.

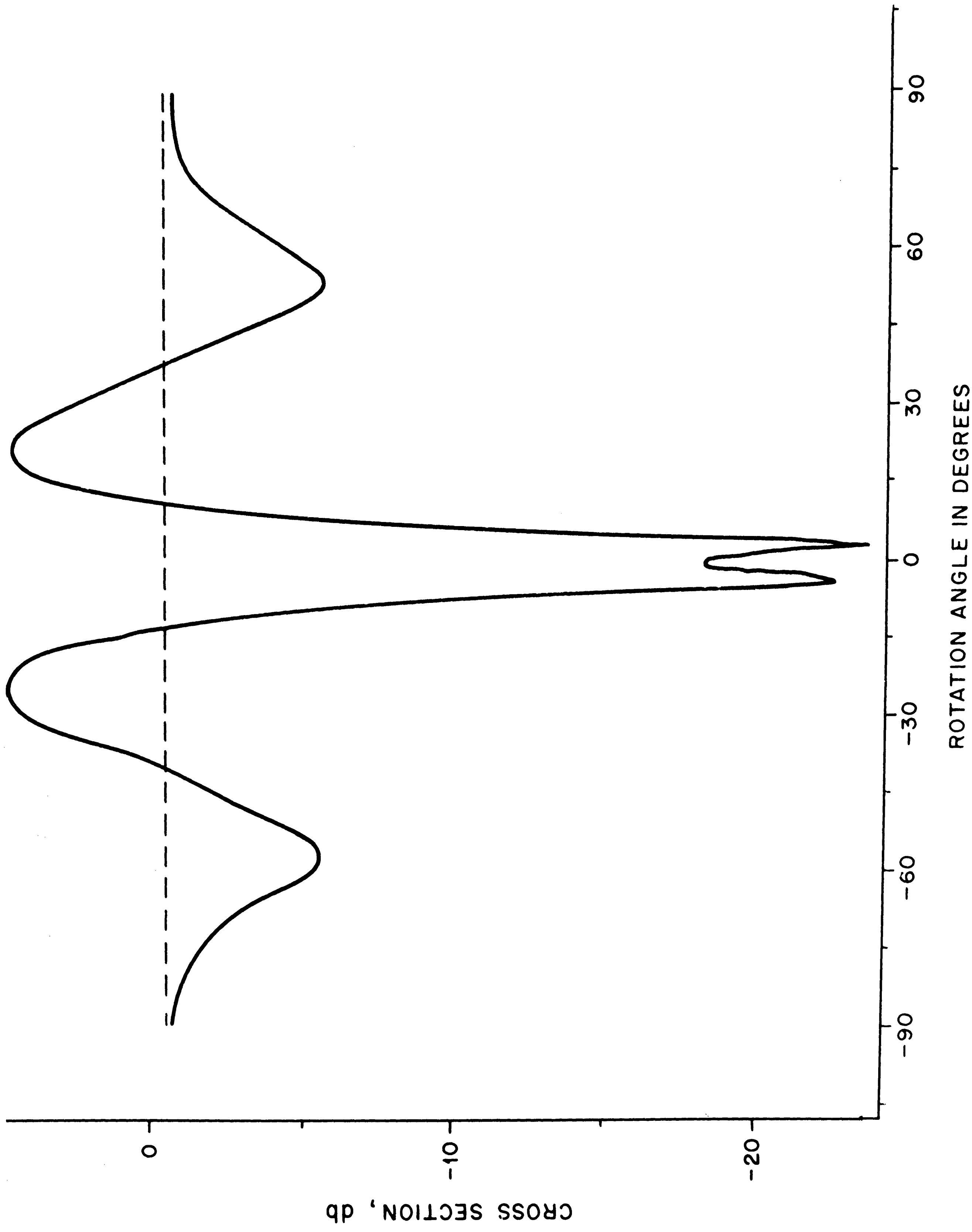

FIG. 27: EXPERIMENTAL BACK SCATTERING CROSS SECTIONS OF LOADED (—) AND UNLOADED (---) SPHERE: ka=4.280, HORIZONTAL POLARIZATION.

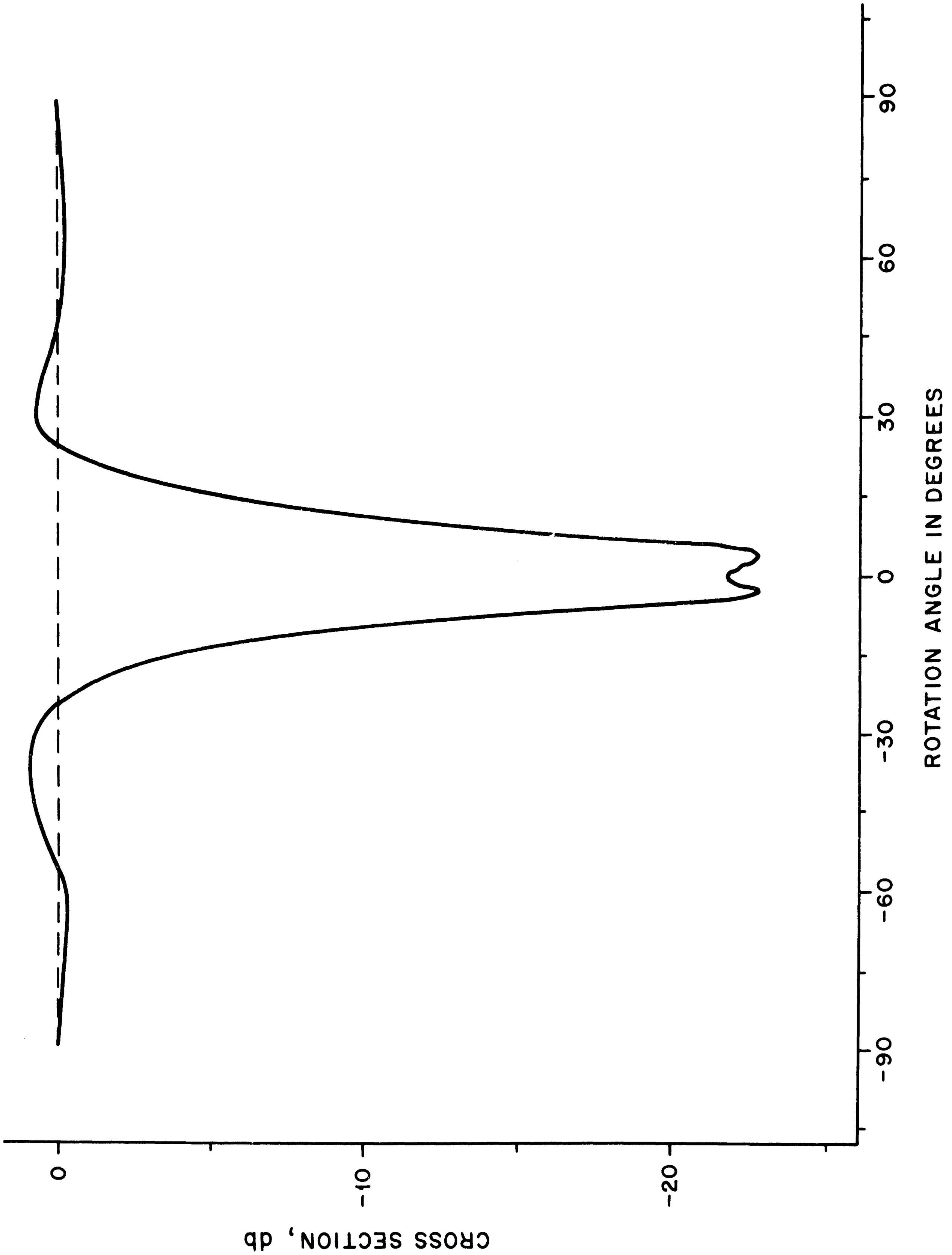

FIG. 28: EXPERIMENTAL BACK SCATTERING CROSS SECTIONS OF LOADED (—) AND UNLOADED SPHERE: ka=4.280, VERTICAL POLARIZATION.

VI
CONCLUSIONS

In the preceding sections we have considered the scattering behavior of a metallic sphere loaded with a slot in the plane normal to the direction of incidence. The slot was assumed to be of small but finite width, with the electric field constant across it, and under this assumption the analysis for the external fields is exact. Expressions for the scattered far field components were derived, which can then be used to investigate the modification to the scattering cross section produced by various types of loading.

The loading admittance necessary for some particular modification is in general complex, with positive or negative real part corresponding to an active or passive load respectively. If attention is confined to the back or forward scattering direction or, for $\theta \neq 0$ or π, to a single* component of the scattered field, it is, perhaps, obvious that there is no limit to the amount by which the cross section in some specified directions can be varied when active slots are allowed. The effectiveness of passive slots, however, may come as more of a surprise, and because of the immediate practical application of passive loading, emphasis has been placed on this case.

For slots at 60^o, 90^o or 120^o the loading required to produce a zero back scattering cross section was computed for $0 < ka \leq 10$ at intervals of 0.1. The variations of the real and imaginary parts are quite complex, but taking just the real part of the loading admittance, we observe that ranges of ka in which Re. Y_ℓ is positive (passive slot) or negative (active slot) alternate with one another. Thus, with a given slot position, passive loading can nullify the return only for certain ranges of ka, but since their limits are functions of θ_o, it is feasible that two (or more) slots could be used to cover much larger ranges within which a null can be achieved. Even outside such a range a passive loading may still provide a significant reduction in cross section. The maximum and minimum cross sections

*With the chosen type of slot there is, in general, no loading either active or passive which will reduce $\sigma(\theta)$ to zero for $\theta \neq 0$ or π.

obtainable with single passive load have been computed for the above values of θ_o and ka, and enhancements by as much as 20 db are not uncommon.

To verify some of these conclusions, a model was constructed with a circumferential slot at $\theta_o = 90^o$ backed by a cavity whose depth could be varied. Since the corresponding loading is susceptive, attention was concentrated on those frequencies at which a change in susceptive loading would produce a marked variation in the back scattering cross section, and for each such frequency the cross section was measured for a series of different shorting discs. Using the theory for an asymmetrically-excited radial cavity, the disc size was related to the loading, and when the resulting values for the modified cross section were compared with the theoretical curves for cross section versus susceptance, excellent agreement was found.

In addition to the choice of loading, we also have at our disposal the location of the slot, and the "optimum" in this regard depends on the type of cross section modification desired. If, for example, it is required to reduce the back scattered returns from small spheres to zero, a displacement of the slot from 90^o to 60^o increases the upper limit of the ka range which can be continuously covered with passive loading, and it seems probable that further reductions in θ_o would increase the range still more. One of the intriguing questions yet unanswered is the value of θ_o at which this improvement in control ceases.

In any application of reactive loading, some of the parameters of practical importance are the bandwidth, the sensitivity of the cross section modification to small changes in the loading, and the angular width in either back scattering or bistatic operation over which the desired reduction or enhancement is achieved. All of these are, of course, functions of ka, θ_o and θ. An indication of the loading sensitivity can be obtained from the afore-mentioned curves of cross section versus susceptive loading, and some estimates of the beamwidth have been determined for the particular case ka = 4.280 and $\theta_o = 90^o$. With a loading such as to give zero back scattering, the calculated width (between 3 db points) of the minimum under bistatic operation was 36^{o} in the E-plane and 60^{o} in the H-plane, and for back scattering (which involves a rotation of the direction of incidence) the corresponding measured widths were 20^{o} and 36^{o} respectively. It is almost certain, however, that these widths could be substantially increased if the loading were selected for maximum beamwidth rather than for a null at $\theta = 0$.

To provide more information about the above parameters, and to obtain more complete bounds on the cross section modifications that are possible, it is necessary to pursue further the computations based on the theoretical solution derived in this report. As part of this continuing study it is our intention to investigate the maximum reduction and enhancement of the total scattering cross section, as well as giving increased attention to modifications in directions other than $\theta = 0$. The solution for arbitrary angles of incidence will also be considered.

ACKNOWLEDGEMENTS

The authors wish to acknowledge the assistance of Mr. J. Ducmanis and Mr. Prakash Sikri who carried out the digital programming and Mr. H. E. Hunter who did the required hand computation.

VIII
REFERENCES

Ås, B.O. and H.J. Schmitt (1958), "Back Scattering Cross Section of Reactively Loaded Cylindrical Antennas," Harvard University, Cruft Lab. Scientific Report No. 18.

Bailin, L.L. and S. Silver (1956), "Exterior Electromagnetic Boundary Value Problems for Spheres and Cones," Trans. IRE-PGAP, AP-4, pp 5-16.

Bechtel, M.E. (1962), "Scattering Coefficients for the Backscattering of Electromagnetic Waves from Perfectly Conducting Spheres," Cornell Aeronautical Lab. Report No. AP/R1S-1.

Chen, K-M (1964a), "Reactive Loading of Arbitrarily Illuminated Cylinders to Minimize Microwave Backscatter," submitted to Can. J. Phys.

Chen, K-M (1964b), "Minimization of Back Scattering of a Cylinder by Double Loading," submitted to IEEE Trans. Ant. and Prop.

Chen, K-M and V.V. Liepa (1964), "The Minimization of the Back Scattering of a Cylinder by Central Loading," IEEE Trans. Ant. and Prop., AP-12, pp 576-582.

Green, R.B. (1963), "The General Theory of Antenna Scattering," The Ohio State University, Report No. 1223-17.

Harrington, R.F. (1963), "Electromagnetic Scattering by Antennas," IEEE Trans Ant. and Prop., AP-11, pp 596.

Harrington, R.F. (1964), "Theory of Loaded Scatterers," Proc. IEE (London), 111, pp 617-623.

Hu, Y-Y (1958), "Backscattering Cross Section of a Center-Loaded Cylindrical Antenna," Trans. IRE-PGAP, AP-6, pp 140-148.

Iams, H.A. (1950), "Radio Wave Conducting Device," U.S. Patent No. 2,578,367.

Kazarinoff, N.D. and T.B.A. Senior (1962), "A Failure of Creeping Wave Theory," Trans. IRE-PGAP, AP-10, pp 634-638.

King, R.W.P. (1956), "The Theory of Linear Antennas," Harvard University Press, Cambridge, Mass.

Plonus, M. A. "On the Impedance of a Finite Slot," to be published.

Schiff, L. I. (1954), "On an Expression for the Total Cross Section," Prog. Theor. Phys., 11, pp 288-290.

Senior, T. B. A. and R. F. Goodrich (1964), "Scattering by a Sphere," Proc. IEE (London), 111, pp 907-916.

Sletten, C. J., P. Blacksmith, F. S. Holt and B. B. Gorr (1964), "Scattering from Thick Reactively Loaded Rods," appearing in AFCRL Report No. 64-727.

Stratton, J. A. (1941), Electromagnetic Theory, McGraw-Hill, New York.

Weinberg, L. (1963), "New Technique for Modifying Monostatic and Multistatic Radar Cross Sections," IEEE Trans. Ant. and Prop., AP-11, pp 717-719.

APPENDIX A
AN EXTREMUM PROBLEM

In Section IV the following extremum problem arises: given

$$\Gamma = \left| 1 + \frac{\gamma_1 + i\gamma_2}{x_1 + i x_2} \right|^2 \tag{A-1}$$

where γ_1, γ_2, x_1 and x_2 are real, find the maximum and minimum values of Γ subject to the condition $x_1 \geq b > 0$.

From Equation (A-1)

$$\Gamma = \frac{(\gamma_1 + x_1)^2 + (\gamma_2 + x_2)^2}{x_1^2 + x_2^2} \tag{A-2}$$

and since there is no restriction on the allowed x_2, we can obtain one condition connecting the x_1 and x_2 for which Γ is a maximum or a minimum by equating $\partial\Gamma/\partial x_2$ to zero. Hence

$$x_2 \left\{ (\gamma_1 + x_1)^2 + (\gamma_2 + x_2)^2 \right\} = (x_1^2 + x_2^2)(\gamma_2 + x_2) \; , \tag{A-3}$$

and the extreme values of Γ are therefore given by

$$\Gamma = 1 + \frac{\gamma_2}{x_2} \; . \tag{A-4}$$

If x_1 is unrestricted it is obvious that

$$\Gamma_{min} = 0$$

corresponding to

$$x_2 = -\gamma_2$$

and, from (A-3),

$$x_1 = -\gamma_1 \; .$$

Similarly,

$$\Gamma_{max} = \infty$$

corresponding to

$$x_2 = x_1 = 0 .$$

On the other hand, if it is required that $x_1 \geq b$, the above extremes may not be achievable. This is true of the minimum if $-\gamma_1 < b$, and of the maximum if $0 < b$. To investigate these cases, equation (A-3) is solved for x_2 as a function of x_1 and the solution inserted into (A-4) to give

$$\Gamma_{min} = 1 + \frac{1}{2x_1^2}\left\{\gamma_1^2 + \gamma_2^2 + 2\gamma_1 x_1 - \sqrt{(\gamma_1^2 + \gamma_2^2 + 2\gamma_1 x_1)^2 + 4\gamma_2^2 x_1^2}\right\} , \quad \text{(A-5)}$$

$$\Gamma_{max} = 1 + \frac{1}{2x_1^2}\left\{\gamma_1^2 + \gamma_2^2 + 2\gamma_1 x_1 + \sqrt{(\gamma_1^2 + \gamma_2^2 + 2\gamma_1 x_1)^2 + 4\gamma_2^2 x_1^2}\right\} . \quad \text{(A-6)}$$

Note that as $x_1 \rightarrow \pm\infty$,

$$\Gamma_{min} \rightarrow 1 + \frac{\gamma_1}{x_1} - \frac{\gamma_1^2 + \gamma_2^2}{x_1} = 1 - O(|x_1|^{-1})$$

$$\Gamma_{max} \rightarrow 1 + \frac{\gamma_1}{x_1} + \frac{\gamma_1^2 + \gamma_2^2}{x_1} = 1 + O(|x_1|^{-1}) .$$

Also, for $x_1 = 0$,

$$\Gamma_{min} = \frac{\gamma_1^2}{\gamma_1^2 + \gamma_2^2} ,$$

$$\Gamma_{max} = \infty ;$$

and for $x_1 = -\gamma_1$,

$$\Gamma_{min} = 0 \ ,$$

$$\Gamma_{max} = \frac{\gamma_1^2 + \gamma_2^2}{\gamma_1^2} \ .$$

A complete schematic of the behavior of Γ_{min} and Γ_{max} as functions of x_1 is as shown in Figure A. 1, and since Γ_{max} is monotonically

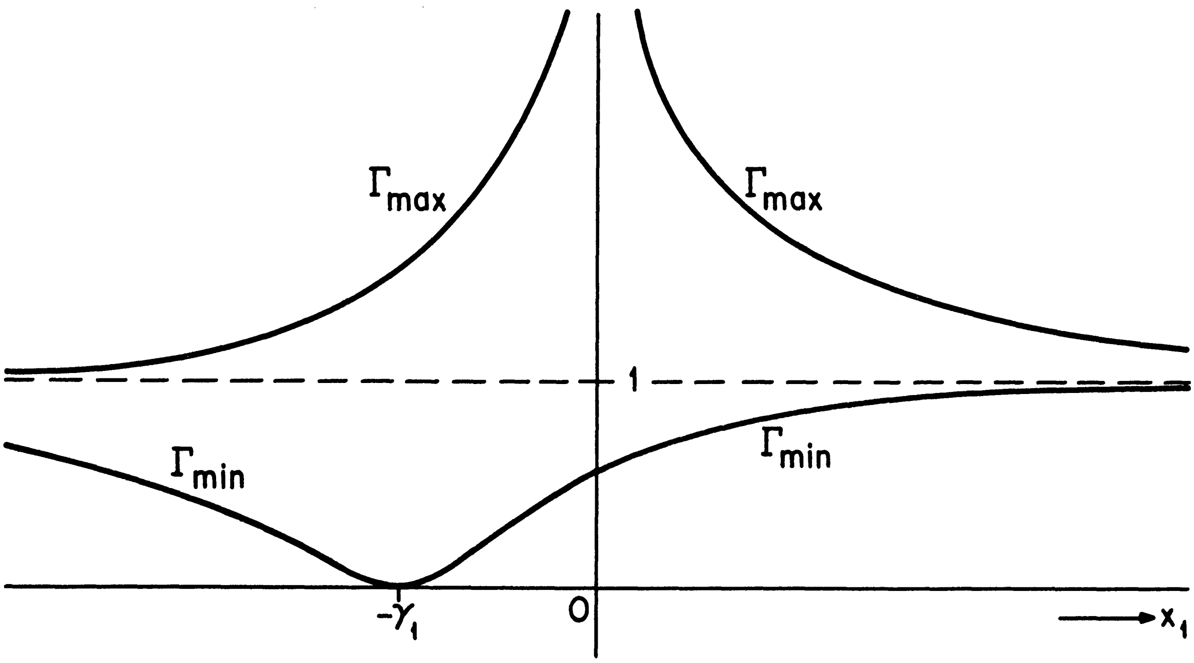

FIGURE A. 1: MAXIMUM AND MINIMUM VALUES OF Γ AS FUNCTIONS OF x_1 (DRAWN FOR $\gamma_1 > 0$).

decreasing as $|x_1|$ increases, whilst Γ_{min} is monotonically increasing as $|x_1+\gamma_1|$ increases, it is now a straightforward matter to specify the extreme values of Γ for $x_1 \geq b$. Thus, if $-\gamma_1 \geq b$,

$$\Gamma_{min} = 0 \tag{A-7}$$

for $x_1 = -\gamma_1$, $x_2 = -\gamma_2$, but if $-\gamma_1 < b$

$$\Gamma_{min} = 1 + \frac{\gamma_2}{x_2}, \tag{A-8}$$

where $x_1 = b$ and

$$x_2 = -\frac{1}{2\gamma_2}\left\{\gamma_1^2+\gamma_2^2+2\gamma_1 b+\sqrt{(\gamma_1^2+\gamma_2^2+2\gamma_1 b)^2+4\gamma_2^2 b^2}\right\}. \tag{A-9}$$

Similarly, if $0 \geq b$,

$$\Gamma_{max} = \infty \tag{A-10}$$

for $x_1 = x_2 = 0$, but if $0 < b$,

$$\Gamma_{max} = 1 + \frac{\gamma_2}{x_2} \tag{A-11}$$

where $x_1 = b$ and

$$x_2 = -\frac{1}{2\gamma_2}\left\{\gamma_1^2+\gamma_2^2+2\gamma_1 b-\sqrt{(\gamma_1^2+\gamma_2^2+2\gamma_1 b)^2+4\gamma_2^2 b^2}\right\}. \tag{A-12}$$

APPENDIX B
THE INPUT ADMITTANCE OF AN ASYMMETRICALLY EXCITED RADIAL CAVITY

In order to use the experimental model of Section V to verify the theoretically predicted scattering behavior of the slotted sphere, it is necessary to relate the input admittance of the cavity to its dimensions and, in particular, to the radius b of the inner conductor. Bearing in mind that the slot is of small width centered on $\theta_o = \pi/2$, it would appear sufficient to regard the cavity as a radial one, and in terms of the cylindrical polar coordinates (r, ϕ, z) where

$$x = r\cos\phi, \qquad y = r\sin\phi, \qquad z = z,$$

the situation is now as shown in Figure B.1.

The cavity is of width $d = a\delta$ and is shorted at $r=b$. At the outer edge $r=a$ it is excited by a voltage $-v\cos\phi$ (the sign difference with respect to the voltage implied by equation (18) is a consequence of the fact that $\hat{z} = -\hat{\theta}$ at $\theta = \pi/2$) and since it is assumed that $d \ll \lambda$, the components E_r and E_ϕ of the electrical field within the cavity can for all practical purposes be neglected. The only remaining E component is then E_z, and this must satisfy the wave equation which, in cylindrical coordinates, is

$$\frac{1}{r}\frac{\partial}{\partial r}(r E_z) + \left(k^2 + \frac{1}{r^2}\frac{\partial^2}{\partial \phi^2}\right)E_z = 0 .$$

The general solution for $0 < b \le r \le a$ is

$$E_z = \sum_{n=-\infty}^{\infty} \left\{ E_n J_n(kr) + F_n N_n(kr) \right\} e^{in\phi} \tag{B-1}$$

where $J_n(kr)$ and $N_n(kr)$ are cylindrical Bessel functions of the first and second kinds respectively, and E_n and F_n are constants to be determined. The boundary conditions on the sides of the cavity are satisfied automatically by (B-1). At the inner and outer surfaces, however, the conditions are

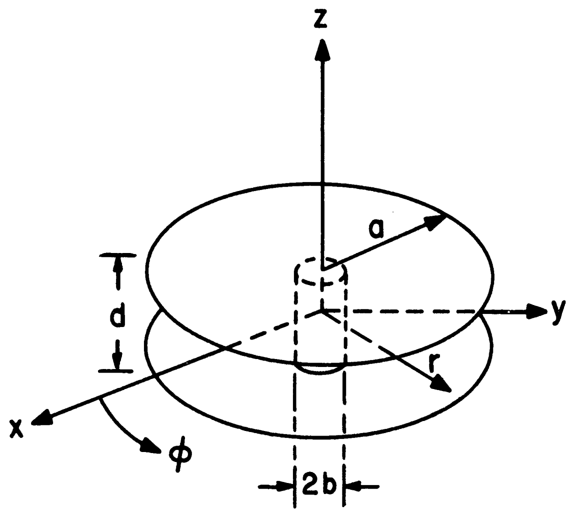

FIGURE B. 1: GEOMETRY OF THE RADIAL CAVITY

$$E_z = 0 \qquad \text{for } r = b$$

$$= \frac{v}{d}\cos\phi \qquad \text{for } r = a \,,$$

and on applying these to (B-1), we obtain

$$E_z = \frac{v}{d}\;\frac{J_1(kr)\,N_1(kb) - N_1(kr)\,J_1(kb)}{J_1(ka)\,N_1(kb) - N_1(ka)\,J_1(kb)}\;\cos\phi \;. \qquad \text{(B-2)}$$

The corresponding circumferential component of the magnetic field can be found from Maxwell's equations, and is

$$H_\phi = -i\,Y\,\frac{v}{d}\;\frac{J_1'(kr)\,N_1(kb) - N_1'(kr)\,J_1(kb)}{J_1(ka)\,N_1(kb) - N_1(ka)\,J_1(kb)}\;\cos\phi \;. \qquad \text{(B-3)}$$

Since both E_z and H_ϕ are functions of ϕ, we shall again employ the concept of admittance density. The power flow across the aperture and into the cavity is

$$w = -\int_{-d/2}^{d/2} \frac{1}{2}(\underline{E} \times \underline{\tilde{H}}) \cdot \hat{r}\, dz$$

$$= \frac{1}{2}\,\frac{v\cos\phi}{d}\int_{-d/2}^{d/2} H_\phi\, dz$$

$$= \frac{1}{2}\, v\cos\phi\, H_\phi \;,$$

from which we have

$$y_\ell = \frac{\left[H_\phi\right]_{r=a}}{v\cos\phi} \;.$$

The total input admittance Y_L follows on integrating this around the circumference of the cavity, and hence

$$Y_\ell = -i\,Y\,2\pi \frac{a}{d}\;\frac{J_1'(ka)\,N_1(kb) - N_1'(ka)\,J_1(kb)}{J_1(ka)\,N_1(kb) - N_1(ka)\,J_1(kb)} \;. \qquad \text{(B-4)}$$

As $b \rightarrow a$

$$Y_\ell \longrightarrow -i\,Y\,2\pi \frac{a}{d} \cdot \frac{1}{k(a-b)} \;,$$

and the admittance therefore approaches $-i\infty$ with decreasing cavity depth. We also remark that if the cavity were filled with a medium of refractive index μ, the expression for the admittance would follow immediately from equation (B-4) on replacing k by μk and Y by the intrinsic admittance of the medium. Thus for real μ, numerical values can be obtained by scaling those for an air-filled cavity.

The expression for Y_ℓ has been programmed for an IBM 7090 computer to give data for any ka and a/d as a function of kb. For the sphere used in the experimental study the diameter was 3.133 inches, the gap width 0.0625 inches, and the spacing discs enabled 2b to be varied in 22 steps from a minimum of 0.3125 inches to 3.133 inches. In order to have the computed data directly applicable to the experimental model, kb was written in the form

$$kb = ka\; \frac{x}{3.133} \;,$$

and the data was printed out for the first 22 values of the inner diameter x (in inches) appropriate to the shorting discs. Because of the infinity when $b = a$, the largest x computed was 3.0. Typical values of the relative admittance $Y_\ell\,/Y$ are shown in Table B.1 for $ka=2.340$, 3.198 and 4.280, corresponding to model frequencies 2.808, 3.838 and 5.136 Gc respectively.

TABLE B.1

x	Im. Y_ℓ/Y		
	ka=2.340	ka=3.198	ka=4.280
0.3125	5.11660×10	2.11267×10^2	-4.54191×10^2
0.5	4.27339×10	1.78511×10^2	-9.35062×10^2
0.625	3.56367×10	1.56155×10^2	-3.99939×10^3
0.75	2.75690×10	1.34651×10^2	1.66094×10^3
0.875	1.86384×10	1.14320×10^2	6.68595×10^2
1.0	8.89309	9.51331×10	4.07230×10^2
1.125	-1.67804	7.68998×10	2.83760×10^2
1.25	-1.31419×10	5.93523×10	2.09659×10^2
1.375	-2.56254×10	4.21876×10	1.58491×10^2
1.5	-3.93243×10	2.50748×10	1.19542×10^2
1.625	-5.45215×10	7.64651	8.75723×10
1.75	-7.16175×10	-1.05244×10	5.96227×10
1.875	-9.11829×10	-2.99670×10	3.37720×10
2.0	-1.14047×10^2	-5.13812×10	8.55957
2.125	-1.41456×10^2	-7.57552×10	-1.73586×10
2.25	-1.75359×10^2	-1.04581×10^2	-4.55074×10
2.375	-2.18995×10^2	-1.40283×10^2	-7.79833×10
2.5	-2.78155×10^2	-1.87146×10^2	-1.18196×10^2
2.625	-3.64329×10^2	-2.53616×10^2	-1.72612×10^2
2.75	-5.03990×10^2	-3.59103×10^2	-2.55854×10^2
2.875	-7.74912×10^2	-5.60545×10^2	-4.10564×10^2
3.0	-1.54720×10^3	-1.12879×10^3	-8.39197×10^2

Unclassified

Security Classification

DOCUMENT CONTROL DATA - R&D

(Security classification of title, body of abstract and indexing annotation must be entered when the overall report is classified)

1. ORIGINATING ACTIVITY *(Corporate author)* University of Michigan Radiation Laboratory	2a. REPORT SECURITY CLASSIFICATION Unclassified 2b. GROUP

3. REPORT TITLE

Modification to the Scattering Behavior of a Sphere by Reactive Loading.

4. DESCRIPTIVE NOTES *(Type of report and inclusive dates)*

Scientific Report No. 2

5. AUTHOR(S) *(Last name, first name, initial)*

Liepa, V. V. and Senior, T. B. A.

6. REPORT DATE October 1964	7a. TOTAL NO. OF PAGES 74	7b. NO. OF REFS 19

8a. CONTRACT OR GRANT NO. AF 19(628)-2374	9a. ORIGINATOR'S REPORT NUMBER(S) 5548-2-T
b. PROJECT NO. 5635	
c. TASK 563502	9b. OTHER REPORT NO(S) *(Any other numbers that may be assigned this report)*
d.	AFCRL-64-915

10. AVAILABILITY/LIMITATION NOTICES

U. S. Government agencies may obtain copies of report from DDC. Other persons and organizations should apply to U. S. Dept of Commerce, Office of Technical Services.

11. SUPPLEMENTARY NOTES	12. SPONSORING MILITARY ACTIVITY Air Force Cambridge Research Laboratories L. G. Hanscom Field, Bedford, Mass.

13. ABSTRACT

Electromagnetic scattering behavior by a metallic sphere loaded with a circumferential slot in the plane normal to the direction of incidence is investigated. The slot is assumed to be of small but non-zero width with electric field constant across it, and under this assumption the analysis of external field is exact. The field scattered in any direction is obtained by superposition of the field diffracted by an unloaded sphere and that radiated by an excited slot at the position of the load, with the radiation strength of the slot related to the loading characteristics in the combined problem. Thus, there are two parameters that determine the scattering behavior of this object: the loading admittance and the position of the slot.

Numerical results are presented primarily for the case of back scattering and these are compared with experimental measurements made using a metallic sphere with an equatorial slot backed by a radial cavity of adjustable depth.

DD FORM 1 JAN 64 1473

Security Classification

Unclassified

Security Classification

14. KEY WORDS	LINK A		LINK B		LINK C	
	ROLE	WT	ROLE	WT	ROLE	WT
Sphere	9	1				
Circumferential Slot	10	2				
Electromagnetic Scattering	8, 5	1				
Reactive Loading	10	1				
Sphere			9	1		
Experimental Data			2	2		
Theoretical Computations			2	2		
Electromagnetic Scattering			8,5	1		
Reactive Loading			10	1		

INSTRUCTIONS

1. ORIGINATING ACTIVITY: Enter the name and address of the contractor, subcontractor, grantee, Department of Defense activity or other organization *(corporate author)* issuing the report.

2*a*. REPORT SECURITY CLASSIFICATION: Enter the overall security classification of the report. Indicate whether "Restricted Data" is included. Marking is to be in accordance with appropriate security regulations.

2*b*. GROUP: Automatic downgrading is specified in DoD Directive 5200.10 and Armed Forces Industrial Manual. Enter the group number. Also, when applicable, show that optional markings have been used for Group 3 and Group 4 as authorized.

3. REPORT TITLE: Enter the complete report title in all capital letters. Titles in all cases should be unclassified. If a meaningful title cannot be selected without classification, show title classification in all capitals in parenthesis immediately following the title.

4. DESCRIPTIVE NOTES: If appropriate, enter the type of report, e.g., interim, progress, summary, annual, or final. Give the inclusive dates when a specific reporting period is covered.

5. AUTHOR(S): Enter the name(s) of author(s) as shown on or in the report. Enter last name, first name, middle initial. If military, show rank and branch of service. The name of the principal author is an absolute minimum requirement.

6. REPORT DATE: Enter the date of the report as day, month, year, or month, year. If more than one date appears on the report, use date of publication.

7*a*. TOTAL NUMBER OF PAGES: The total page count should follow normal pagination procedures, i.e., enter the number of pages containing information.

7*b*. NUMBER OF REFERENCES: Enter the total number of references cited in the report.

8*a*. CONTRACT OR GRANT NUMBER: If appropriate, enter the applicable number of the contract or grant under which the report was written.

8*b*, 8*c*, & 8*d*. PROJECT NUMBER: Enter the appropriate military department identification, such as project number, subproject number, system numbers, task number, etc.

9*a*. ORIGINATOR'S REPORT NUMBER(S): Enter the official report number by which the document will be identified and controlled by the originating activity. This number must be unique to this report.

9*b*. OTHER REPORT NUMBER(S): If the report has been assigned any other report numbers *(either by the originator or by the sponsor)*, also enter this number(s).

10. AVAILABILITY/LIMITATION NOTICES: Enter any limitations on further dissemination of the report, other than those imposed by security classification, using standard statements such as:

(1) "Qualified requesters may obtain copies of this report from DDC."

(2) "Foreign announcement and dissemination of this report by DDC is not authorized."

(3) "U. S. Government agencies may obtain copies of this report directly from DDC. Other qualified DDC users shall request through
________________."

(4) "U. S. military agencies may obtain copies of this report directly from DDC. Other qualified users shall request through
________________."

(5) "All distribution of this report is controlled. Qualified DDC users shall request through
________________."

If the report has been furnished to the Office of Technical Services, Department of Commerce, for sale to the public, indicate this fact and enter the price, if known.

11. SUPPLEMENTARY NOTES: Use for additional explanatory notes.

12. SPONSORING MILITARY ACTIVITY: Enter the name of the departmental project office or laboratory sponsoring *(paying for)* the research and development. Include address.

13. ABSTRACT: Enter an abstract giving a brief and factual summary of the document indicative of the report, even though it may also appear elsewhere in the body of the technical report. If additional space is required, a continuation sheet shall be attached.

It is highly desirable that the abstract of classified reports be unclassified. Each paragraph of the abstract shall end with an indication of the military security classification of the information in the paragraph, represented as *(TS)*, *(S)*, *(C)*, *or (U)*.

There is no limitation on the length of the abstract. However, the suggested length is from 150 to 225 words.

14. KEY WORDS: Key words are technically meaningful terms or short phrases that characterize a report and may be used as index entries for cataloging the report. Key words must be selected so that no security classification is required. Identifiers, such as equipment model designation, trade name, military project code name, geographic location, may be used as key words but will be followed by an indication of technical context. The assignment of links, rules, and weights is optional.

Unclassified

Security Classification